CR-152254

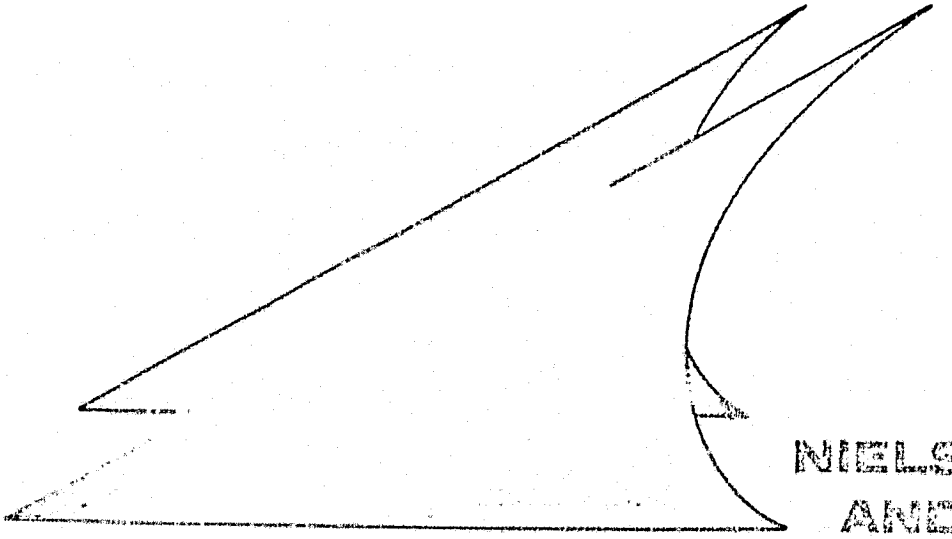

NIELSEN ENGINEERING AND RESEARCH, INC.

OFFICES: 510 CLYDE AVENUE / MOUNTAIN VIEW, CALIFORNIA 94043 / TELEPHONE (415) 968-9457

THEORETICAL ANALYSIS OF AN AUGMENTOR WING FOR A VTOL FIGHTER

Marnix F. E. Dillenius
and
Michael R. Mendenhall

NEAR TR 183

May 1979

Prepared under Contract NAS2-9605

for

NATIONAL AERONAUTICS AND SPACE ADMINISTRATION
Ames Research Center

NIELSEN ENGINEERING & RESEARCH, INC.
510 Clyde Avenue, Mountain View, CA 94043
Telephone (415) 968-9457

TABLE OF CONTENTS

THEORETICAL ANALYSIS OF AN AUGMENTOR WING FOR A VTOL FIGHTER

by Marnix F. E. Dillenius and Michael R. Mendenhall

SUMMARY

An analytical method has been developed for predicting forces and moments acting on augmentor wings in hover or forward flight for prescribed ejector jet characteristics. The method is based on incompressible, potential flow theory. Attached flow is assumed. Two potential flow models are incorporated in the prediction method: a model for the wing/flap system and a model for the jet and its wake. A three-dimensional nonplanar vortex lattice is laid out on the chordal planes of the augmentor wing components. Flap surfaces and jet can be at large angles to the oncoming stream. Horseshoe vortex strengths are determined from the application of the flow tangency condition at points on the surfaces including interference effects from the jet. The jet is made to expand from the primary nozzles to the diffusor exit, and a distribution of vorticity is placed on the jet boundary to model entrainment. In addition, blockage panels are positioned on the boundary of the jet wake downstream of the augmentor wing. Jet wake centerline location and spreading rate are taken from experimental data. The solution proceeds in an iterative manner using the two flow models in sequence and comparing the predicted diffusor exit velocity with the specified velocity.

Experimental data involving VTOL fighter-type augmentor wings are not readily available; however, some comparisons are shown using data on a V/STOL transport model in forward flight. Good agreement is shown at low thrust settings. For high thrust settings, the present method overpredicts the overall lift and drag and underpredicts the pitching moment. The discrepancy is at least partly attributable to the attached flow assumption.

INTRODUCTION

There has been an increasing interest in the development of VTOL high performance aircraft. One concept used to achieve VTOL capability is the augmentor wing. In this concept, the propulsion system is integrated with the lifting surfaces for generating direct lift. The augmentor wing of interest here consists of a fixed wing with a set of large flap surfaces at the trailing edge which can be deflected at large angles to guide and control the engine exhaust gas. The gas or primary jet emanates from nozzles at the trailing edge of the center flap positioned above the forward and aft flaps designed to form a diffusor or ejector system. In this process, the jet entrains secondary air drawn into the diffusor and mixes with it resulting in an augmentation in mass flow. As a result, the overall thrust is larger than the primary thrust generated by the engine exhaust diverted from the engine to the augmentor wing. Furthermore, additional lift is generated by the wing and flap system due to interference effects induced by the augmented jet flow.

The objective of this report is to describe an analytical method developed for the prediction of the external aerodynamic characteristics of an augmentor wing for specified jet velocities at the primary jet nozzle and the diffusor exit. Flow conditions include hover and forward flight. This effort is a necessary precursor to the prediction of the longitudinal aerodynamic forces and moments acting on a complete VTOL-type fighter aircraft with one or more augmentor wing systems. The work performed during this phase was funded jointly by NASA and NAVAIR.

Several analytical methods based on jet flap theory have been developed to analyze wind-on performance of augmentor wings. Two-dimensional approaches are given in references 1 through 4. The thin jet flap theory is not a realistic model for the "thick" augmentor wing jets. Bevilaqua, reference 5, presents a two-dimensional analysis for the static (wind-off) case using a viscous solution for the flow through the diffusor and an inviscid solution for the external flow. The viscous inner flow solution is based on a turbulence kinetic energy model to account for mixing. Very recently, the inner solution was extended to account for hyper-mixing nozzles (ref. 6). Bevilaqua's methods can predict details of the jet flow inside the diffusor including average jet velocities at the exit of the diffusor.

The present method is directed towards the three-dimensional case of a finite-aspect-ratio wing with sweep and taper having a highly deflected, thick augmentor jet. It is desirable, as well, to account for spanwise variation of the jet width and jet velocities for a realistic three-dimensional case. The approach consists of developing models for the wing-flap system and those aspects of the augmentor jet that are required to properly model the interference effects of the jet on the wing-flap loading. The details of the flow inside the augmentor and the mixing of the primary and secondary flows are not addressed, and the augmentor jet characteristics are assumed to be prescribed initially in terms of parameters which yield the primary jet velocity and the mixed flow velocity at the ejector exit. Potential flow methods are employed, and no flow separation on the wing or flap surfaces is assumed to occur.

Recently, a Navy fighter prototype employing an augmentor canard and wing was built and tested. It is designated XFV-12A and is described in reference 7. No test data is readily available for this configuration. The basic features, including the augmentor wing systems, are indicated in figure 1. In order to evaluate the methods and provide some comparisons with data, calculations were made on a rectangular, finite-aspect-ratio V/STOL transport configuration for which wind tunnel data are available (ref. 8). Unlike the fighter configuration, the transport wing has a short chord and high thickness ratio and the flap segments also have high thickness ratios. A cross section of the configuration is shown in figure 2. Results are presented on this configuration, and discussion is presented on the flow and load characteristics as illuminated by the comparisons between prediction and data.

SYMBOLS

AR	aspect ratio
b	width of jet measured perpendicular to jet center
C_A	axial force coefficient, axial force/qS_{REF}, figure 3
C_m	pitching moment coefficient, pitching moment/$qS_{REF}\ell_{REF}$, figure 3
C_N	normal force coefficient, normal force/qS_{REF}, figure 3
C_μ	jet momentum coefficient, eqn. (9)
$\bar{c}$	average wing chord
$\vec{F}$	aerodynamic force vector
ℓ_{REF}	reference length, $\ell_{REF} = \bar{c}$
M	mass flow rate
m_p	jet mass flow rate at jet exhaust
m_s	entrained air mass flow rate
$\vec{n}$	vector normal to surface
q	dynamic pressure
$\vec{q}$	resultant flow velocity vector
S	length along jet centerline
S_{REF}	reference area
T	thrust force
V_∞	free stream velocity
v	flow velocity
x,y,z	wing coordinate system, figure 3
α	angle of attack, degrees
δ	flap deflection angle, degrees, figure 2
$\vec{\Gamma}$	vortex vector with strength Γ
γ	vorticity strength/unit length
ϕ	thrust augmentation ratio
ξ	nondimensional length along jet centerline

SYMBOLS (Concluded)

CG	center of gravity
$\mathfrak{L}$	jet centerline
E	diffusor exit
I	initial (at center flap exhaust nozzle location)
j	jet

TECHNICAL APPROACH

The basic objective of the analytical method is to represent the solid surfaces of the augmentor wing by a distribution of lifting-type singularities for the purpose of calculating aerodynamic loads including jet interference effects. To this end, the jet must be represented by suitable singularities from its origin to some distance downstream of the diffusor in order to model the jet induced effects. A nonplanar vortex lattice is laid out on the augmentor wing components. This lifting surface model is basically a modified form of the vortex lattice approach described in reference 9. The vortex distribution used to model the jet over its length is an adaptation of the jet model used in the work described in references 9 and 10. In addition, the jet wake (jet downstream of the diffusor exit) makes use of blockage panels on its boundary. This part of the jet model is an extension of the blockage panel scheme described in reference 11.

The lifting surface and jet models have been programmed and are used in sequence to form an iterative approach to the calculation of the longitudinal aerodynamic characteristics (lift, drag, pitching moment) of augmentor wing configurations. In this process, the assumption is made that flow entrainment by the primary jet is such that the flow at the diffusor exit is completely mixed. This condition, to a first approximation, is approached in practice when hyper-mixing primary nozzles are employed in conjunction with limited boundary layer blowing.

In the following sections, brief descriptions are given of the lifting surface and the jet flow models. Attention will be focused on the special features developed to apply the flow models to augmentor wings. The iteration scheme is described in the section concerned with the method of solution.

Vortex-Lattice Model for Augmentor Wing/Flaps System

General description.- The vortex-lattice lifting-surface model used to represent the solid surfaces is a modified version of the model used in reference 9. Configurations of interest in that reference comprise externally blown flaps attached to the trailing edge of a wing. In the present investigation, the computer program of reference 9 was extended to handle flaps typical of augmentor wing/flap systems, as shown in

figures 2 and 3. Each component is covered with horseshoe vortices on its mean surface. The trailing legs of the horseshoe vortices are made to lie in, and extend to infinity in the plane of each surface. However, the trailing legs of the horseshoe vortices on the wing (or that surface of the augmentor wing ahead of the forward flap) are bent at the wing trailing edge so that they lie in the plane of the forward flap as illustrated in figure 3.

The wing/flap geometric parameters and flow conditions taken account of in the present methods are summarized below. More detailed descriptions are given in reference 9. The wing may have

- finite span
- breaks in sweep of the leading and trailing edges
- uniform dihedral over the span
- taper set by leading- and trailing-edge shapes
- twist and camber
- zero wing thickness only

Up to 10 flap surfaces can be accounted for. The description of the planform of the flaps is governed by the following geometric characteristics.

- partial span
- straight leading- and trailing-edge shapes over the span
- taper set by leading- and trailing-edge sweeps
- root chord in plane parallel to vertical or x-z plane, see figure 3
- tip chord must lie in a vertical plane parallel to the vertical plane containing the root chord
- twist and camber
- zero flap thickness only

Effects of angle of sideslip and compressibility are not included. Angle of attack, flap deflection angle, dihedral angle, twist and camber angles are accounted for in the flow tangency condition using trigonometric functions since some of these angles can be large.

Vortex layout.- A few horseshoe vortices and the reference coordinate system (x,y,z) are shown in figure 3 for a tapered augmentor wing/flap system with swept leading- and trailing-edges. The flaps are set at large deflection angles typical of hover and transition flight. An

augmentor diffusor section is formed by the forward and aft flaps. The chordal planes of the wing, center flap, and diffusor flaps are divided into trapezoidal area elements or panels. On the forward flap, the spanwise distribution of the panels must be the same as on the wing. A horseshoe vortex is placed in each panel such that the bound (or spanwise) leg lies along the panel quarter chord and the trailing legs lie along the side edges of the panel. The trailing legs extend back to infinity in the plane of the panel except for the horseshoe vortices on the wings. The legs originating on this surface trail back to the trailing edge and are then bent to lie in the plane of the forward flap. In fact, the wing trailing legs will coincide with the trailing legs of the horseshoe vortices on the forward flap. Figure 3 shows one horseshoe vortex only on the chordal planes of the wing, forward flap, center flap and aft flap. On the forward flap the trailing legs associated with the wing vortices are shown slightly separated from the trailing legs of the horseshoe vortices of the forward flap for the purpose of clarity. The strengths of the horseshoe vortices, unknown so far, are obtained from the flow tangency condition described next.

Boundary condition.- The flow tangency boundary condition is applied at control points located at the midspan of the three-quarter chord line of each area element or panel. Details are given in reference 9, pages 9 through 14. A brief account only is given here. Some control points are indicated on figure 3. Designate the total resultant velocity vector at one control point as $\vec{q}$ and the normal to the surface in question as $\vec{n}$, then the boundary condition states

$$\vec{q} \cdot \vec{n} = 0 \tag{1}$$

for the finite set of control points. With no jet present, velocity $\vec{q}$ includes contributions from all the horseshoe vortices laid out over the augmentor wing surfaces and the free stream component. The velocity components induced by the horseshoe vortices are related to the unknown vortex strengths through the use of influence functions given in reference 9. The functions associated with horseshoe vortices on the wing account for the effects of the angle of deflection of the trailing legs. In the application to augmentor wings, velocity contributions induced by the jet singularities are included in equation (1) for the purpose of accounting for jet interference. A later section concerned with the jet

model describes the method used to generate the jet induced velocity contributions. Note that the free stream component represents the flight condition: hover (zero velocity), transition or forward flight (nonzero).

The application of the flow tangency condition, equation (1), at the control points distributed over the chordal planes of the augmentor wing surfaces results in a set of simultaneous equations from which the unknown vortex strengths are obtained. Once the strengths are known, the aerodynamic forces and moments acting on the augmentor wing components are calculated using the method described next. At this stage it is also possible to compute, at any field point, the flow field induced by the horseshoe vortices representing the surfaces of the augmentor wing.

Forces and moments.- The aerodynamic forces acting on one elemental area or panel can be determined from the application of the Kutta-Joukowski law for forces acting on a vortex filament. The fundamental statements are given in reference 12. This approach has been used successfully in references 9 and 10 and others. Details of the application of the vortex filament force method are discussed in reference 9, pages 17 and 18. A summarized account only will be given here.

The aerodynamic force acting on a vortex filament per unit length of filament is expressed as the vector product of the velocity of the flow $\vec{q}$ past the vortex of strength $\vec{\Gamma}$.

$$\vec{F} = \vec{q} \times \vec{\Gamma} \tag{2}$$

Contributions from all horseshoe vortices laid out over the augmentor wing components, free stream and jet induced contributions are included in the calculation of $\vec{q}$. The elemental panel force calculated with equation (2) can be used to compute spanwise load distributions by summing over all the panels and overall pitching moments are determined by using the panel forces times the appropriate moment arms. The results include normal force, axial force and pitching moment coefficients. The directions of the normal and axial force coefficients, C_N and C_A, respectively, are shown in figure 3.

Jet Model Including Jet Wake

The analytical singularity distribution chosen to represent the external induced effects of the jet is described in this section. The jet, exhausting from the trailing edge of the center flap (figure 3), is divided into two distinct regions for modeling. The first region is that portion of the jet from its exhaust nozzle to the exit of the diffusor. Secondary jets are not included in the present analysis. The second region is the remainder of the jet from the diffusor exit to its chosen end point at a finite distance downstream of the exit. The following is a description of the details of this jet model.

General approach.- The objective of the jet model is to represent the induced external flow effects of the jet, ignoring the details of the mixing flow inside the diffusor and the internal flow of the initial region of the jet. The basic flow model used as a starting point for the required jet model is that of an actuator disk which can be used to represent a jet of fluid with higher velocity and higher total head than the surrounding fluid. This flow model has been used to represent the external flow field induced by the wake from a turbojet or turbofan engine (refs. 9 and 10). In reference 9, the development of the flow model for circular and elliptic cross section jets is described, and in reference 10, the extension of this model to a rectangular cross section jet is presented. The latter rectangular jet model is the most appropriate model for the application to augmentor wings.

The equivalent singularity distribution for an actuator disk is a semi-infinite length cylinder with a uniform distribution of vorticity on its surface (ref. 13). Two characteristics of this model are a uniform velocity profile inside the jet and an increasing mass flow within the boundary over the initial few diameters of length. This model has been extended to expanding boundaries, various cross sectional shapes, and bent centerlines for use as a turbojet wake model. In making these modifications, the analytical singularity model of a uniform vorticity distribution on a semi-infinite cylinder was changed to a finite length distribution of vortex rings. This change was necessitated by numerical difficulties in calculating the induced velocity field associated with the singularity distribution for curved jets, and more details of this change are presented in reference 10.

The above mentioned singularity distribution will be adapted to the current problem of developing a jet model for an augmentor wing. Downstream of the augmentor, the jet should behave as a free jet and thus can be handled in the same manner as the previous jet wake models. The upstream region of the jet model, in the diffusor region, is quite different from previous jet models. For the case at hand, the jet exhausts from a very high aspect ratio slot nozzle at the trailing edge of the center flap and expands very rapidly to fill the diffusor. In this process the jet entrains air drawn into the diffusor. The assumption is made that the jet and entrained air are completely mixed and fill the diffusor exit. The rates of expansion and entrainment of secondary fluid by the jet are much larger than typical free jet rates because of the enhanced mixing over the relatively short length of the diffusor. Therefore, a new flow model is required in this region. This is described in the following sections.

Diffusor region.- This portion of the jet model, between the center flap trailing edge exhaust nozzle and the end of the diffusor section, is quite different from the jet models described in references 9 and 10. The major difference is the high rate of expansion of the jet boundaries due to the mixing in the diffusor. In actual practice, the mixing process is enhanced by the use of hyper-mixing nozzles and boundary layer blowing on the inner surfaces of the diffusor. The entrainment rate of the jet is therefore much higher than that of a free jet because of the mass augmentation effect of the diffusor. In this context, the fluid entrained by the jet is assumed to be the entire amount of secondary fluid; that is, the entrained flow is the difference between the total mass flow at the diffusor exit and the jet mass flow at the primary nozzle.

The boundaries of the jet in the diffusor region are shown dashed in figures 3 (and 6). Since the present model is not concerned with the details of the internal flow, the idealized boundaries are prescribed by straight line segments as shown. The only requirement is that the jet model expand to fill the exit at the end of the diffusor. The initial portion of the jet is sized to match the actual cross sectional area of the jet nozzle at the center flap. The short length of nonexpanding boundaries near the trailing edge of the center flap, shown in figures 3 (and 6) is included to give the analytical jet model an initial run length to build up to the correct jet velocity. This length is typically

four or five times the minimum cross section dimension, in this case, the width of the jet. Since details of the actual jet in the diffuser are unknown, the jet boundary is specified to expand linearly to the exit of the diffusor after the initial run length, and the centerline of the jet is positioned approximately midway between the forward and aft flaps. The spanwise dimension of the jet is assumed constant; therefore, the width of the jet is the only changing dimension. This results in a decreasing cross-section aspect-ratio along the length of the jet in the diffusor. A schematic of the jet model, to be used later, is shown in figure 4(a).

The distribution of vorticity, γ, along the length of the jet boundary is determined in the following manner. The initial vorticity strength at the primary jet nozzle is specified from the known value of primary nozzle mass flow velocity v_{j_I} to be

$$\gamma_I = v_{j_I} \tag{3}$$

This vorticity strength per unit length remains constant in the initial region to give the centerline velocity an opportunity to stabilize at the correct value. Since the jet model does not attempt to model the distribution of velocity inside the diffusor, the next point at which jet mass flow is known is at the diffusor exit. At this station the vorticity strength per unit length is specified to be

$$\gamma_E = v_{j_E} \tag{4}$$

where v_{j_E} is the flow velocity associated with the total mass flow at the end of the diffusor.

The distribution of vorticity between the initial and exit values was examined using two different methods. The first method is a linear variation of strength between the two known values. The local vorticity strength is given by the relation

$$\gamma = \gamma_I - \left(\frac{s - s_I}{s_E - s_I}\right)\left(\gamma_I - \gamma_E\right) \tag{5}$$

as illustrated in figure 4(b). This distribution was abandoned after some preliminary calculations. The discontinuity in the slope of the strength curve at each end caused certain difficulties in the calculation

of the induced velocities inside the jet boundary. The induced velocities on the centerline could not stabilize at the appropriate initial and exit values because of the rapid change in vortex strength occurring at the beginning and end of the linear region.

The second approach to the specification of the vorticity between γ_I and γ_E uses a ninth-order polynomial distribution. It is defined as

$$\frac{\gamma - \gamma_E}{\gamma_I - \gamma_E} = a\xi^9 + b\xi^8 + c\xi^7 + d\xi^6 + e\xi^5 + f\xi^4 + g\xi^3 + h\xi^2 + i\xi \qquad (6)$$

where

$$\xi = \frac{S_E - S}{S_E - S_I} \qquad (7)$$

We require that the first three derivatives of $\frac{\gamma - \gamma_E}{\gamma_I - \gamma_E}$ with respect to ξ be zero at $S = S_I$ and the first six derivatives be zero at $S = S_E$. In this way, the vorticity is concentrated towards the jet exhaust. This is necessary to model the high jet-flow velocity at the exhaust nozzle and allows for high entrainment rates over the length of the diffusor. Equation (6) becomes

$$\frac{\gamma - \gamma_E}{\gamma_I - \gamma_E} = 28\xi^9 - 63\xi^8 + 36\xi^7 \qquad (8)$$

which produces smooth centerline velocity distributions between S_I and S_E for any values of γ_I and γ_E.

Centerline velocity distributions for two thrust levels are shown in figure 5. From the end of the initial region of the jet to the end of the diffusor region, the velocity is very smooth and well behaved. The predicted velocity in the initial region is typical of the results obtained with this jet model.

One comment can be included at this time regarding the possibility of calculating the strength of the vorticity distribution which will produce a specified centerline velocity distribution. This approach was examined with partial success. If the expansion of the jet is moderate, for example, if $b_E = 4b_I$ (b is the jet width), then this inverse procedure works very well. It does have the disadvantage that velocities must be specified at a large number of points on the centerline, but this can be handled by curve fitting or assuming a distribution of velocities.

When the expansion is much larger, numerical difficulties arise which prevent a reasonable solution for the vorticity strengths. These difficulties stem from an ill conditioned matrix in which the diagonal terms are not dominant. The results indicate an erratic distribution of vorticity which do not produce a realistic external velocity field. For this reason, this approach was abandoned in favor of the method employing the ninth-order polynomial distribution.

Downstream region.- The portion of the jet model in the region downstream of the diffusor exit is treated as a free jet wake. The length of the jet is chosen to be sufficiently long so that any further increase in length does not affect appreciably the flow velocities predicted by the jet model at the exhaust nozzle and the diffusor exit. The vorticity distribution on the wake boundary is held constant at the value γ_E specified at the end of the diffusor, which is the requirement for a free jet model (ref. 10). The remainder of the jet is specified in a manner similar to the procedure presented in reference 11.

The wake cross section is rectangular over the entire length of the wake, but the boundary is allowed to expand according to available empirical information. Holding the span of the wake constant, the spreading information contained in reference 11 is applied to the wake width. The effect of an expanding boundary does not have a large effect on the induced loading on the wing and flap surfaces; therefore, this approximate approach for setting the spreading rate is considered adequate for the current investigation.

The path taken by the jet after it leaves the end of the diffusor must be specified with respect to the location of the diffusor exit. This is done using empirical information on the path of a rectangular jet in a crossflow (ref. 14). Small differences in the centerline path do not create large differences in the induced loading on the lifting surfaces; therefore, based on the success of a similar approach in reference 11, the empirical data of reference 14 are used for all calculations included in this report. The jet wake boundaries are shown in figure 6a for the case $v_{j_E}/V_\infty = 4$ and in figure 6b for $v_{j_E}/V_\infty = 1.4$.

The final component of the jet wake model in the downstream region is the blockage model. It is well known that a jet exhausting into a crossflow behaves as if the jet boundary is nearly a solid surface. To approximate this effect, the surface of the wake is represented by a

finite number of vortex quadrilateral panels with a control point at the panel centroid as shown in figure 6. The boundary condition of no flow through the control point on each panel results in a set of simultaneous equations. The velocity to be canceled at the blockage panel control points consists of a contribution of the free stream to which are added the perturbation velocity components induced by the vortex lattice on the wing/flap system with power off. This has the effect of allowing the blockage panels to be porous to the fluid entrained by the distribution of vorticity modeling the wake (as well as the jet). It also takes account, in the first approximation, of the effects caused by the augmentor wing on the jet wake. The blockage panel or quadrilateral vortex strengths are then determined from the simultaneous equations. Velocities induced by the blockage panels will be included in the calculation of the power-on horseshoe vortex strengths of the wing/flap system at a later stage.

Method of Solution

The flow models discussed above have been implemented in computer programs which are arranged to be used in a sequential manner. This arrangement was found to be convenient in the iteration scheme used to arrive at a solution. In a series of steps, the vortex lattice and jet analysis are applied as follows:

Step 1. The vortex lattice analysis is applied to the augmentor wing surfaces without jet induced effects in the boundary condition. The power-off horseshoe vortex strengths are determined. Velocities induced by the horseshoe vortices at the control points of the blockage panels are computed.

Step 2. The jet wake centerline and boundaries are located. Blockage panel strengths are calculated using velocities induced by the power-off horseshoe vortex lattice with strengths determined in step 1. At this point the blockage portion of the jet wake model has been modeled. The blockage-induced effects at the control points on the wing/flaps surfaces are calculated and will be used in a later step.

Step 3. The jet model is now applied to the augmentor jet for purposes of calculating the distribution of vorticity within the augmentor and downstream of the augmentor exit. As noted previously, the vorticity distribution is determined by the jet velocity at the exhaust nozzle of the center flap and at the diffusor exit. These are specified from the augmentor performance prescribed initially for the calculation. The assumption is made that these velocities are produced only by the distribution of vorticity representing the jet, and the vorticity distribution is calculated. The jet-induced velocities at the wing/flap control points are calculated.

Step 4. The vortex lattice analysis is applied again to the augmentor wing surfaces. This time, the boundary condition includes velocity components induced by the distribution of vorticity and the blockage panels modeling the jet and its wake. The horseshoe vortex strengths are recalculated. Next, the flow field at the diffusor exit is computed including contributions generated by the vortex lattice on the wing/flap system, the distribution of vorticity and the blockage panels modeling the jet, and the component of the free stream (zero for the hover case). The area averaged flow velocity is determined and compared with the specified diffusor exit average velocity.

At this stage, the predicted value is usually higher in magnitude than the specified value. A lower diffusor exit velocity is selected and fed back to the jet analysis, step 3. All other input is kept the same including jet exhaust velocity, centerline location, and spreading rates inside and downstream of the diffusor region. For the same horseshoe vortex lattice and blockage panel layout, step 3 is repeated with the adjusted diffusor exit velocity for the jet analysis. A new vortex distribution is computed for the jet and the induced velocity components at the wing/flap control points are updated. Step 4 is repeated and the average flow velocity at the diffusor exit recomputed. If the updated value matches the specified one within a selected error bound, the iteration is stopped. The forces and moments calculated by the horseshoe vortex analysis now reflect the effects of the mutual

interference between the jet and the augmentor wing surfaces and the effect of the free stream. The overall forces and moments are calculated as the sum of the contribution from the jet itself (thrust at the exhaust nozzle) and the contribution from forces acting on the horseshoe vortex lattice representing the wing/flaps system.

It should be noted that the specified velocities at the exhaust nozzle (at the trailing edge of the center flap) and the diffusor exit should be for the actual flow conditions at hand. As such, the specified diffusor exit velocity deduced from experimental data (or directly measured) is already representative of the presence of the augmentor wing surfaces and especially the effects of the actual jet wake. Therefore, as long as the iteration scheme described above results in a predicted flow velocity at the diffusor exit that matches the specified value, the location and shape of the jet wake is not of primary importance in the calculation of the forces and moments. In other words, under these conditions the jet wake has a small effect on loads. The region of the jet inside the diffusor, through its large entrainment effect, is mainly responsible for the interference effects of the jet on the aerodynamic loads acting on the augmentor wing surfaces. Finally, it is noted that this procedure not only produces the correct mass flow at the center flap nozzle exit and the diffusor exit, but the correct secondary flow entering the diffusor.

THEORETICAL RESULTS AND COMPARISONS

Partially due to the newness of the augmentor wing concept and partially for proprietary reasons, very limited experimental data involving augmentor wing configurations are in the public domain. In particular, component loading and pressure distribution data on a VTOL fighter-type configuration such as shown in figure 1 are practically unavailable. There is probably more data available for static (zero forward velocity) conditions. Even though the methods described in this report can handle the static (or hover) case, it was more important to test the methodology with forward flight conditions because of the emphasis placed on developing a lifting surface modeling scheme, accounting for jet interference effects, applicable to VTOL fighter-type augmentor wings in flight.

The only data made available to test the augmentor wing analysis described herein involves the wind tunnel transport model of reference 8. This model is shown in figure 7. A cross section of its rectangular augmentor wing system is indicated in figure 2 for a set of flap deflection angles representative of transition conditions. Inherently, this model does not resemble a VTOL fighter type, figure 1, in that the augmentor wing system is unswept and thick in section. Compared to the streamwise flap lengths, the forward or wing part is extremely short. In addition, the model employs a fuselage with considerable cross section area atypical of a VTOL fighter. Furthermore, figure 2 shows secondary jet nozzles on the forward and aft flap components. In VTOL fighter configurations, these jets serve to control the boundary layers on the diffusor walls formed by the forward and aft flap surfaces. The amount of engine exhaust diverted to the secondary nozzles may vary. For the transport model under consideration, the size of the secondary nozzles in the forward and aft flaps indicate that appreciable amounts of exhaust air could be diverted to them. References 8 and 15 do not contain information about the division of flow between the primary and secondary nozzles.

In spite of the somewhat unsuitable geometric characteristics of the wind tunnel model described above and the uncertainty in the division of flow between the primary and secondary jet nozzles, the theoretical methods were applied to this configuration for preliminary verification and to point out the usefulness of the methods for indicating areas of improvement in the preliminary design stages of augmentor wings.

In what follows, the layout of the horseshoe vortices on the surfaces of the augmentor wing under consideration is described. Then, based on the assumption that the flow out of the secondary nozzles is small compared to the flow from the primary nozzle, the jet centerline and boundary positions are specified and the blockage panel layout is given for two power settings. Some of the calculated flow fields induced by the vortex lattice alone and jet alone will be shown. They are the results of the intermediate steps described in the section entitled "Method of Solution". As a result of the iteration, the adjusted diffusor exit velocities input to the jet model are given, and final velocity distributions calculated by the present method at the exit are shown. Finally, comparisons are made between the predicted and measured overall forces and moments.

Panel Layout on Surfaces

The horseshoe vortex lattice layout on the surfaces of the augmentor wing for use in the comparisons with data obtained with the transport model shown in figure 7 will now be described. As can be seen on that figure, the model includes a fuselage and a tail section. The former will only be partially accounted for by the present method but the latter (horizontal tail) is represented by an additional horseshoe vortex lattice to be solved simultaneously with the vortex lattice on the surfaces of the augmentor wing. Thus, as far as the model components are concerned, the augmentor wing system and horizontal tail will be handled by the present methods including an approximation for the lift carried over on to the fuselage. Flow conditions include zero angle of attack and two forward flight speeds.

Chordal planes.- The wing, forward flap, center flap, and aft flap components of the augmentor wing system, shown in figure 2, are idealized to the chordal plane representation shown in figure 6. The wing/flap components are extended through to the fuselage centerline to account for body lift carryover. However, the jet is made to span only over the exposed wing/flap region and the effects of the jet are felt by the surfaces in that region only (i.e., no jet effects are included on the part of the augmentor wing surfaces inside the fuselage). In this way, the lift carryover onto the fuselage is accounted for to first order for both power-on and power-off conditions. At the present time, the methods cannot account for the effects of the fuselage (Beskin upwash) on the augmentor wing surfaces. Therefore, flow conditions including nonzero angle of attack introduce uncertainty with the present method when a fuselage is part of the configuration under consideration.

Symmetry.- It should be noted that because of geometrical and flow symmetry about the vertical plane through the fuselage centerline, only one half of a given configuration need be covered with a vortex lattice. In fact, the transport wind-tunnel model under consideration here is a half model mounted on the tunnel wall for the same reasons.

Number of horseshoe vortices.- For all comparisons discussed later, the augmentor wing surfaces on one side of the vertical plane of symmetry will be treated as follows. In the chordal plane of the wing of the rectangular wing/flap system, shown in cross section in figure 6, 11

horseshoe vortices are laid along the span and three along the chord. On the forward flap, the spanwise number is the same but four horseshoe vortices are laid out on the chord because of the longer length involved. On the center flap, the spanwise number is also 11, and three are placed along the chord. The aft flap, with the longest chord length, is covered by 11 spanwise and five chordwise horseshoe vortices. As a consequence, there are 33 horseshoe vortices on the wing, 44 on the forward flap, 33 on the center flap and 55 on the aft flap. Note that the trailing legs of the horseshoe vortices on the wing are bent at the wing trailing edge to lie in the chordal plane of the forward flap. This construction is also indicated for the one horseshoe vortex on the wing of the general augmentor wing system of figure 3. Finally, the horizontal tail is covered by an additional horseshoe vortex lattice consisting of five vortices along the span and three along the chord. Thus, a total of 180 horseshoe vortices represent the augmentor wing/flaps and horizontal tail. Their strengths are determined from one set of simultaneous equations as described in an earlier section.

Layout of Jet Boundaries and Blockage Panels, and Jet Induced Velocities

For the case at hand, the jet and jet wake are to be modeled for two power settings using the method described above in the section concerned with the jet model. The power settings are expressed as the thrust or jet momentum coefficient, C_μ, associated with the jet at the exhaust nozzle located at the trailing edge of the center flap. The assumption is made that the secondary nozzles have negligible effect.

$$C_\mu = \frac{T}{qS_{REF}} = \frac{Mv_{j_I}}{qS_{REF}} \tag{9}$$

In the above expression, T is the thrust force produced at the trailing edge of the center flap, M is the mass flow rate and, v_{j_I} is the exhaust nozzle mass flow velocity referred to earlier in equation (3). Comparisons with experimental data from reference 8 will be discussed for C_μ = 1.5 and 7.31. Note that due to symmetry, the effects of the jet on the opposite side of the vertical plane of symmetry must be accounted for. At the present time, the mutual interference between the left and right jets is not included in the analysis.

Layout inside diffusor.- Consider the chordal plane representation, shown in figure 6, of the rectangular augmentor wing of figures 2 and 7. The boundaries of the portion of the jet inside the diffusor formed by the forward and aft flaps is indicated by the dashed line in figure 6. It is based on the procedure described earlier concerned with the diffusor region. The "exit" location is defined by the location along the straight jet centerline where the jet boundaries reach their maximum width. This position is also marked on figures 4(a), 5 and 6. Referring to figures 6(a) and 6(b), the coordinates of the centerline and the width b of the jet inside the diffusor are the same for both power settings and are specified below. For the jet on the left side of the plane of symmetry, the geometrical characteristics are given in the following table.

x		y		z		b/2	
cm	(in)	cm	(in)	cm	(in)	cm	(in)
-20.27	(-7.98)	-96.58	(-38.025)	-3.71	(-1.46)	0.30	(0.12)
-21.59	(-8.5)	↓	↓	-1.22	(-0.48)	0.30	(0.12)
-29.49	(-11.61)	↓	↓	13.67	(5.38)	10.29	(4.05)
-31.01	(-12.21)	↓	↓	16.51	(6.50)	10.29	(4.05)
-32.51	(-12.8)	↓	↓	19.35	(7.62)	10.29	(4.05)

As can be seen from the above table and figure 6, the jet boundaries do not expand over the initial run length. This is for the purpose of building up the correct primary jet velocity v_{j_I}. Then, the jet boundary is made to expand linearly to the "exit" of the diffusor. This "exit" location was chosen to coincide approximately with the taps of a total pressure rake used in the tests described in reference 8. Also note that in this layout the forward jet boundary meets the trailing edge of the forward flap.

In the spanwise direction, the jet and jet wake are positioned from the side of the body out to the midspan of the chordwise row of horseshoe vortices at the tip of the augmentor wing. Locating the outboard side face of the jet (and its wake) inboard from the side edges in this way avoids undue influence at the blockage panels control points induced by the strong vorticity along the side edges of the wing and flaps. For the case at hand, the spanwise dimension of the jet is 142.37 cm (56.06 in.).

Input velocities for jet model.- Once the geometrical layout of the jet inside the diffusor region is defined, the primary jet velocity and the velocity of the fully mixed (augmented) jet at the diffusor exit must be specified. In addition, the blockage panels on the jet wake are exposed to a certain flow field as will be discussed later in this section. For the two thrust coefficients, the following table contains the required velocities divided by the free stream. They were calculated using the ideal gas relationship and certain assumptions about pressures and temperatures at the jet nozzle and diffusor "exit" as explained below.

C_μ	ϕ	$\frac{m_s}{m_p}$	v_{j_I} $\frac{cm}{sec}$ $\left(\frac{ft}{sec}\right)$	v_{j_E} $\frac{cm}{sec}$ $\left(\frac{ft}{sec}\right)$	V_∞ $\frac{cm}{sec}$ $\left(\frac{ft}{sec}\right)$	$\frac{v_{j_I}}{V_\infty}$	$\frac{v_{j_E}}{V_\infty}$
1.50	1.28	3.9	25390 (833)	4298 (141)	3048 (100)	8.33	1.41
7.31	1.48	4.7	32248 (1058)	7407 (243)	1905 (62.5)	16.94	3.89

At the primary nozzle exhaust the static pressure was assumed to be 101356.5 newtons/m^2 (14.7 psia). The total temperature in the primary nozzle flow was assumed to be 15.56°C (60°F). From reference 8, enclosure 18, the total-to-static pressure ratios for the primary jet are specified as 1.5 and 2.0 for C_μ = 1.5 and 7.31, respectively. The free stream dynamic heads associated with these two thrust coefficients are 569.77 newtons/m^2 (11.9 lbs/ft^2) and 221.21 newtons/m^2 (4.62 lbs/ft^2), respectively. Density at the diffusor exit was taken equal to free stream density. The diffusor exit velocities, v_{j_E} (shown above), require knowledge of the secondary or entrained mass flow rate m_s and primary nozzle flow rate m_p. Reference 15, page 687, contains a curve relating the mass flow ratio, m_s/m_p, to the thrust augmentation ratio. The thrust augmentation ratio, ϕ, is given in reference 8, enclosure 20, for the two thrust coefficients listed above.

The above mentioned mass flow rates are for the actual flow conditions at hand and include the effects of jet flow issuing from the primary and secondary nozzles. The average diffusor exit velocities are determined

from these data. Thus, even though the analysis assumes that all the exhaust gas is diverted to the primary nozzle, the use of the above exit velocities guarantees that the measured amount of entrainment is accounted for in the present method.

The values given above for the jet velocity at the primary nozzle exit and the diffusor exit will be used in the determination of the distribution of vorticity in accordance with equation (8). As noted earlier in the section describing the stepwise method of solution, the diffusor exit velocity will require adjustment during the successive jet calculations in the iteration process. The values given in the above table for the two power settings will be used as the initial choice.

Wake centerline locations and spreading rates.- For the case at hand, the empirical procedure described in an earlier section under the heading "Downstream region" is applied. The jet centerline location is obtained for the two diffusor exit velocity ratios shown in the previous table from equation (1) of reference 14, which is based on experimental data. The aspect ratio of the jet in a crossflow associated with the cited reference is four, whereas the aspect ratio of the augmentor jet is approximately seven. Therefore, the centerline paths obtained for the two power settings using the data of reference 14 are only approximate. However, in accordance with the arguments given at the end of the section entitled "Method of Solution", the coordinates of the jet aft of the diffusor section need not be very accurate as long as the diffusor exit velocity used in the prediction scheme is directly measured or deduced from data for the configuration and flow conditions at hand.

The cross section of the jet wake is rectangular. Proceeding downstream, the width of the wake expands but the dimension in the spanwise direction is held constant. This latter assumption should be sufficiently adequate for the large aspect ratio (AR = 7) of the augmentor jet under consideration. Reference 11, figure 9, contains information from which the expansion rates are obtained for the two diffusor exit velocity ratios indicated in the previous table for the two power settings. Note that the remarks made above with regard to the accuracy apply to the expansion rates as well. The following tables contain the coordinates of the centerline and the width of the jet wake for the two power settings. Quantity b is the width of the jet wake. Figure 6 shows the coordinate system and the jet wake on the left side of the plane of

symmetry in accordance with the coordinates given in the tables below.

$C_\mu = 1.5$

x		y		z		b/2	
cm	(in.)	cm	(in.)	cm	(in.)	cm	(in.)
-35.05	(-13.80)	-96.58	(-38.025)	23.37	(9.20)	10.90	(4.293)
-38.79	(-15.27)	↓	↓	28.78	(11.33)	12.04	(4.739)
-45.06	(-17.74)	↓	↓	35.53	(13.99)	13.48	(5.306)
-51.33	(-20.21)	↓	↓	40.92	(16.11)	14.40	(5.670)
-57.61	(-22.68)	↓	↓	45.49	(17.91)	15.74	(6.197)
-63.88	(-25.15)	↓	↓	49.48	(19.48)	16.31	(6.423)
-70.15	(-27.62)	↓	↓	53.04	(20.83)	16.93	(6.666)
-76.43	(-30.09)	↓	↓	56.25	(22.15)	17.45	(6.869)
-82.70	(-32.56)	↓	↓	59.23	(23.32)	17.96	(7.071)
-88.98	(-35.03)	↓	↓	61.98	(24.40)	18.25	(7.184)
-95.25	(-37.50)	↓	↓	64.54	(25.41)	18.64	(7.338)

$C_\mu = 7.31$

x		y		z		b/2	
cm	(in.)	cm	(in.)	cm	(in.)	cm	(in.)
-34.80	(-13.70)	-96.58	(-38.025)	23.37	(9.20)	10.90	(4.293)
-38.79	(-15.27)	↓	↓	30.25	(11.91)	12.14	(4.779)
-45.06	(-17.74)	↓	↓	39.70	(15.63)	14.09	(5.549)
-51.33	(-20.21)	↓	↓	48.11	(18.94)	15.95	(6.278)
-57.61	(-22.68)	↓	↓	55.70	(21.93)	17.59	(6.926)
-63.88	(-25.15)	↓	↓	62.66	(24.67)	18.93	(7.452)
-70.15	(-27.62)	↓	↓	69.11	(27.21)	20.37	(8.019)
-76.43	(-30.09)	↓	↓	75.11	(29.57)	21.81	(8.586)
-82.70	(-32.56)	↓	↓	80.75	(31.79)	22.94	(9.032)

For both power settings, the spanwise extent of the jet and its wake is 142.37 cm (56.06 in.).

Blockage panels layout.- The length of the jet wake (measured along the centerline) is taken as approximately three times the chord length of the forward flap, see figure 6. Calculations presented in reference 9 in connection with externally blown flaps indicate that greater jet lengths produce very small changes in aerodynamic loadings at the expense of additional computer time. The blockage of the jet boundaries is modeled by quadrilateral vortex panels described as follows.

On the front and rear faces of the jet wake, ten blockage panels are laid out in the spanwise direction and seven panels in the lengthwise direction. The sides of the jet wake are covered with four blockage panels in the direction normal to the centerline and seven panels are laid out in the lengthwise direction. Thus, the boundaries of the jet wake on the left hand side of the plane of symmetry are covered by 196 panels. To preserve symmetry, the same jet wake and its singularity layout is positioned on the right hand side of the symmetry plane.

The velocity field to be counteracted by the jet wake blockage panels is shown in figure 8 in a vertical plane for part of the jet length. In accordance with step 1 of the section headed "Method of Solution", the flow velocities are generated by the vortex lattice laid out on the surfaces of the augmentor wing and include the free stream velocity. The flow vectors indicated in figure 8 are calculated by the vortex lattice described earlier in connection with the horseshoe vortex paneling layout (180 horseshoe vortices) on the lifting surfaces. Flow conditions are zero degrees angle of attack and zero power setting. Note that the flow velocities at the blockage panel control points are directed downwards. Since the vortex lattice and blockage panel strengths are solved for separately, the flow field seen by the jet wake should be generated by the horseshoe vortices as influenced by the jet. As a first approximation, the power-off horseshoe vortex strengths are used and in the succeeding steps of the iterative approach the blockage panel strengths are kept constant. This constraint can be relaxed and the flow field impressed on the jet wake recalculated once the jet singularities are known. At this time, for the sake of economy the former approach is adopted.

Velocities induced by jet model.- In order to provide some understanding of the entrainment properties of the jet, it is instructive to discuss briefly the flow field induced by the jet model at points

on the components of the augmentor wing. For the jet centerline and boundary locations given in the above tables, the induced flow field in a plane parallel to the x-z plane for the higher ($C_\mu = 7.31$) power setting is shown in figure 9. The directions of the flow vectors at the control points on the forward and aft flaps and the diffusor entrance indicate strong inflow or entrainment towards the initial or narrow part of the jet near the trailing edge of the center flap. In addition, the flow inside the jet at the diffusor exit is fairly uniform and the average velocity ratio (v_{j_E}/V_∞) at the diffusor exit is about 3.8. Note that at this stage the effects of the horseshoe vortices are not included in the diffusor exit velocities.

Predicted Velocity Distributions at Diffusor Exit

The augmentor wing of the transport model shown in figure 7 (and with more detail in figure 2) is modeled by the paneling layouts and jet model specified above. The stepwise procedure described in an earlier section entitled "Method of Solution" is then applied. At the end of the first pass through that procedure, the flow velocities across the diffusor exit are computed as the sum of the vortex lattice and jet-singularities-induced velocities added to the free stream. For both power settings, the predicted velocities at the exit were higher than the specified average flow velocity. In accordance with step 4 of the solution procedure, the diffusor exit velocity, serving as one of the velocity inputs to the jet model, is reduced and the jet model rerun (step 3). The adjusted jet singularity strengths and induced velocities, such as shown in figure 9, are then used in step 4. At the end of step 4, the diffusor exit velocities are calculated again and compared with the specified average flow velocity. When the predicted average diffusor exit velocity matches (to within a certain margin) the specified one, the solution is considered to be converged.

For the $C_\mu = 1.5$ and 7.31 power settings, the following table contains the final input velocities for the jet model and the average of the predicted and specified diffusor exit velocities. The last quantities have been discussed earlier in the section entitled "Layout of Jet Boundaries and Blockage Panels, and Jet Induced Velocities".

	specified and used as initial input to jet model		used as final input to jet model		Vortex lattice + jet model
C_μ	$\left.\frac{V_{j_I}}{V_\infty}\right\|_{initial}$	$\left.\frac{V_{j_E}}{V_\infty}\right\|_{initial}$	$\left.\frac{V_{j_I}}{V_\infty}\right\|_{final}$	$\left.\frac{V_{j_E}}{V_\infty}\right\|_{final}$	$\left.\frac{V_{j_E}}{V_\infty}\right\|_{calc.}$
1.50	8.33	1.40	8.33	0.70	1.46
7.31	16.94	3.89	16.94	3.40	3.83

The calculated flow velocity at the diffusor exit, $\frac{V_{j_E}}{V_\infty}$, is obtained from the area-averaged distribution of flow velocities shown in figure 10(a) for $C_\mu = 1.5$ and in figure 10(b) for $C_\mu = 7.31$, respectively. Note that these velocities are generated by the vortex lattice, the jet vorticity and jet wake blockage panels and include a component of the free stream. The velocity vector associated with the free stream is also shown. The distribution of flow velocities across the diffusor exit is seen to be fairly uniform in accordance with the assumption made to that effect in the description and specification of the jet model. Reference 8 contains some total pressure data obtained with a rake located at the diffusor exit for one spanwise station. The distributions of flow velocities deduced from that data are not uniform and in fact show peaks near the diffusor walls formed by the inner surfaces of the forward and aft flaps. In the tests of reference 8, additional jets issue from the leading edges and are directed along the inner walls of the diffusor for boundary layer control. It is possible, therefore, that the rake measurements are influenced by these secondary jets which are not accounted for in the present method.

The agreement between the calculated diffusor exit flow velocity and the specified value shown in the table above is quite good. At this (final) stage, the forces and moments computed by the vortex lattice method should be representative of the augmentor wing loading including the effects of the jet.

Force and Moment Comparisons

Lift, drag and moment coefficients are shown as a function of thrust or jet momentum coefficient C_μ in figures 11(a), 11(b), and 11(c), respectively, for zero angle of attack. The open symbols are values measured on the complete configuration shown in figure 7 for the set of flap deflection angles specified. The closed symbols represent calculated values for C_μ = 0.0, 1.5 and 7.31 obtained with the paneling layout and jet specification described above for the same flap deflection angles. Only the augmentor wing and horizontal tail surfaces are accounted for in the present method; therefore, any effects from the fuselage on the aerodynamic loads are not included in the calculated values. As far as the drag is concerned, the theory calculates the induced (due to lift) drag contribution only.

At the zero and lower (C_μ = 0.0, 1.5) power settings, the agreement between measurement and theory is good. At the highest moment coefficient (C_μ = 7.31) the lift and drag coefficients are overpredicted and the pitching moment is underpredicted. Overall, the predictions show similar trends as the experiment for increasing thrust coefficient.

Reference 8 contains a few chordwise pressure distributions for one spanwise location for the selected flap settings. Especially at the higher power setting, flow separation is indicated on the center and aft flap. The experimental pressure distribution along the upper surface of the wing and forward flap components (see figure 2) indicate strong suction pressures aft of the secondary nozzle. Similar behavior is indicated at the leading edge of the aft flap on the surface ahead of the secondary nozzle. These observations and the nonuniform measured total pressure across the diffusor exit discussed earlier seem to indicate strong blowing out of the secondary nozzles. This behavior makes itself felt more strongly at the higher power setting since the total pressure distribution at the diffusor exit is shown to be more uniform for the C_μ = 1.5 case. Thus, the partial separation and the strong effects of the secondary nozzles at the higher power setting (C_μ = 7.31) may account for the discrepancy between theory and experiment for that condition.

When interpreting the aerodynamic forces acting on the individual flap surfaces of the augmentor wing system, it is often helpful to analyze the flow field in which these components are immersed. The

present method is capable of determining these flow fields. If, for a given wing/flap segment, the oncoming flow field is at a large angle to it, partial flow separation over that surface would be expected to occur and subsequent loss of lift may result.

As an example of a flow field around the augmentor wing at the same flap deflection angles, consider figure 12. Flow vectors are shown for the case of zero power. It is seen that the wing is subjected to an average upwash of about 15°. The center flap is immersed in a flow field at about 90° to it, and is likely to suffer from flow separation and its consequences on "lift". It is interesting to note that the aft flap is immersed in flow largely aligned with it thus reducing its lift effectiveness. Upstream of the forward flap, there appears to be a low velocity recirculation region. Note that at as much as two chord lengths upstream, strong interference effects are predicted by the present method.

CONCLUDING REMARKS

A method has been developed for determining the external aerodynamics of VTOL fighter-type augmentor wings in hover or transition flight for prescribed ejector jet characteristics. Specifically, the flow velocity at the primary nozzle and an average velocity at the diffusor exit must be prescribed for the flight condition at hand. The augmentor wing may have sweep and taper. The method is based on potential flow theory and attached flow is assumed.

Basically, horseshoe vortex lattice theory is used to represent the solid surfaces of the augmentor wing components. Effects of the jet are included in the flow tangency condition. The jet is modeled by a distribution of vorticity on its boundary. In addition, blockage panels are placed on the jet boundaries downstream of the diffusor exit. Inside the diffusor, the jet model is made to expand from the primary nozzle width to the full width of the diffusor exit as seen in sideview. The jet model accounts for entrainment of secondary air. For given primary nozzle and diffusor exit jet velocities, the aerodynamic loadings acting on the augmentor wing are obtained as the result of an iteration scheme which produces a calculated average diffusor exit flow velocity to match the specified one in magnitude. The iteration scheme consists of a serial application of the vortex lattice and jet model methods.

Experimental data suitable for testing the developed theoretical methods are scarce and/or very difficult to acquire. Some comparisons with experimental data taken with a V/STOL transport model equipped with an unswept and untapered augmentor wing are shown. This configuration is not representative of a VTOL fighter in that the streamwise sections of the augmentor wing components are very thick and it appears that the division of exhaust gas flow between the primary nozzle and secondary nozzles is not representative. At the present time, the method can only accommodate a primary jet issuing from the trailing edge of the center flap located above the diffusor. Consequently, the assumption was made that all the engine exhaust is fed to the primary nozzle. The actual transport model was idealized to chordal plane representations of the augmentor wing components and horizontal tail. Effects of the fuselage are accounted in part only. With these simplifications, the present method calculates lift, drag and pitching moments which agreed well with the experimental data at low power settings. For the higher power setting, the lift and drag are overestimated and the pitching moment is underestimated; however, the predictions show the same trends as experiment for increasing thrust.

With all the engine exhaust assumed to emanate from the primary nozzles, the total entrainment by the single jet is made to be the same as in the case when the power is divided into primary and secondary nozzles. As a result, the calculated overall forces and moments should be representative but detailed information such as component loadings require more knowledge about the flow division.

Notwithstanding the above mentioned limitations, the usefulness of the present method includes the capability of indicating potential problem areas during preliminary design of an augmentor wing system. The developed methods can be used to map the flow field in the vicinity of the augmentor wing for determining interference on other components of the aircraft. In addition, the flow field impressed on each of the flap surfaces of the augmentor wing system can be analyzed so that secondary nozzles for boundary control can be positioned and sized on the basis of that knowledge. Furthermore, the present method can be applied to an existing configuration for which component loads have been measured. By comparing the component load prediction with measurement, components suffering from flow separation and stall can be identified and remedies effected.

On the basis of the work performed so far, the following recommendations are offered.

1. To validate the present method further, additional comparisons should be made with available data for different flap settings and nonzero angle of attack. Component load comparisons should be made. The majority of the engine exhaust should be applied to the primary nozzles for comparison purposes.

2. Detailed data should be taken with a XFV-12A type augmentor wing and made available for testing the developed method.

3. Based on the outcome of 1 and 2, the single augmentor wing system model can be improved by studying effects of different jet boundary layouts and jet vorticity distributions (affecting entrainment) inside the diffusor. Also, the effects of the jet wake on overall and component loads should be determined.

4. It is possible to circumvent the specification of experimentally deduced jet velocities at the primary nozzle and the diffusor exit. Detailed internal flow analyses have been developed elsewhere (ref. 6) capable of generating the required quantities for the jet model of the present method.

5. The present method can be extended to account for more than one jet, i.e. to handle secondary jets and account for the associated Coanda effects on the aerodynamic loads acting on the augmentor wing components. The applicable technology has been developed in connection with USB (Upper Surface Blowing) work described in reference 10.

6. The present method can be extended to account for augmentor canard/augmentor wing systems attached to a fuselage, accounting for mutual interference between the canard, wing, and fuselage.

Nielsen Engineering & Research, Inc.
Mountain View, California 94043
December 1978

REFERENCES

1. Spence, D. A.: The Lift on a Thin Airfoil with a Jet Augmented Flap. Aeronautical Quarterly, Vol. 9, August 1958.

2. Spence, D. A.: The Lift Coefficient of a Thin Jet Flapped Wing. Proc. of Roy. Soc., of London, Ser. A, Vol. 238, No. 1212, Dec. 1956, pp. 46-68.

3. Wilson, J. D., Chandra, S., and Loth, J. L.: Thrust Augmented Wing Sections in Transition Flight. AIAA Paper 75-169, Jan. 1975.

4. Wilson, J. D., Loth, J. L., and Chandra, S.: Thrust Augmented Wing Sections in Potential Flow. West Virginia University, TR-25, Aug. 1974.

5. Bevilaqua, P. M., DeJoode, A. D.: Viscid/Inviscid Interaction Analysis of Thrust Augmenting Ejectors. Interim Report, ONR-CR212-249-1, Feb. 28, 1978.

6. Bevilaqua, P. M.: Optimization of Hypermixing Nozzles. Paper given at the ONR-NAVAIR Contractors Review. Nov. 28-29, 1978. Proceedings to be published.

7. Lewis, E. L., CDR.: XFV-12A, Thrust Augmented Wing (TAW) Prototype Aircraft. Paper given at the Workshop on Thrust Augmenting Ejectors held at Ames Research Center Co-sponsored by NASA/Ames, NADC and AFFDL, June 28-29, 1978, Ames Research Center, Moffett Field, CA 94035.

8. White, E. R.: Experimental and Theoretical Analysis of Augmentor Diffusor Effectiveness on Transport Model (TPA 210, Task 0010). Rockwell International Internal Letter 511-38-75, March 1975.

9. Mendenhall, M. R., Spangler, S. B., Nielsen, J. N. and Goodwin, F. K.: Calculation of the Longitudinal Aerodynamic Characteristics of Wing-Flap Configurations with Externally Blown Flaps. NASA CR-2705, Sept. 1976.

10. Mendenhall, M. R. and Spangler, S. B.: Calculation of the Longitudinal Aerodynamic Characteristics of Upper-Surface-Blown Wing-Flap Configurations. NASA CR-3004, 1978.

11. Perkins, S. C., Jr. and Mendenhall, M. R.: A Correlation Method to Predict the Surface Pressure Distribution on an Infinite Plate from which a Jet is Issuing. NASA CR-152,160, May 1978.

12. Milne-Thomson, L. M.: Theoretical Aerodynamics. Fourth Edition, Section 4.4, Dover Publications, Inc., 1973.

13. Küchemann, D. and Weber, J.: Aerodynamics of Propulsion. McGraw-Hill Book Co., Inc., 1953.

14. Thames, F. C. and Weston, R. P.: Properties of Aspect Ratio 4.0 Rectangular Jets in a Subsonic Crossflow. AIAA Paper No. 78-1508, Aug. 21, 1978.

REFERENCES (Concluded)

15. Stewart, V. R., White, E. R., and Palmer, W. E.: Aerodynamic Analysis of an Integrated V/STOL Thrust Augmentor Lift System Concept. Proceedings of a Workshop held at Institute for Defense Analysis, Arlington, VA, July 1975. Prediction Methods for Jet V/STOL Propulsion Aerodynamics, Vol. II, Editor: M. F. Platzer, Naval Postgraduate School, Monterey, CA.

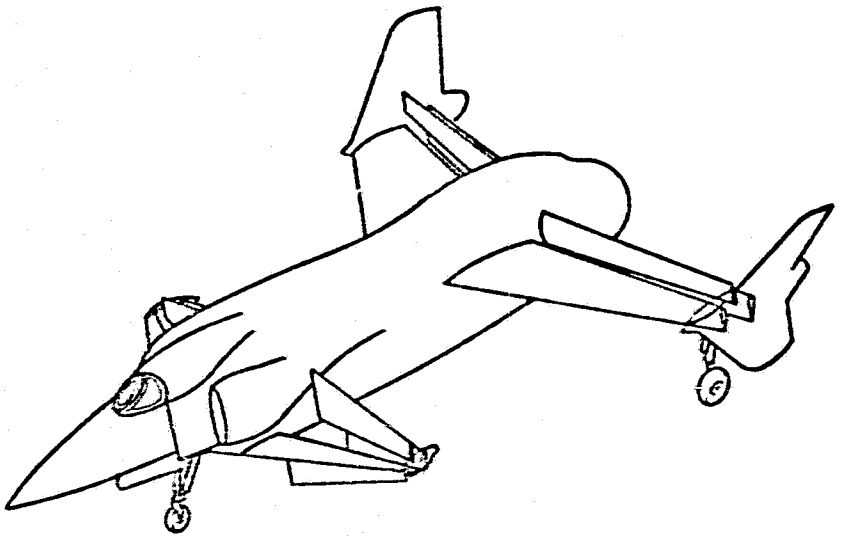

Figure 1.- VTOL fighter with augmentor canard and wing.

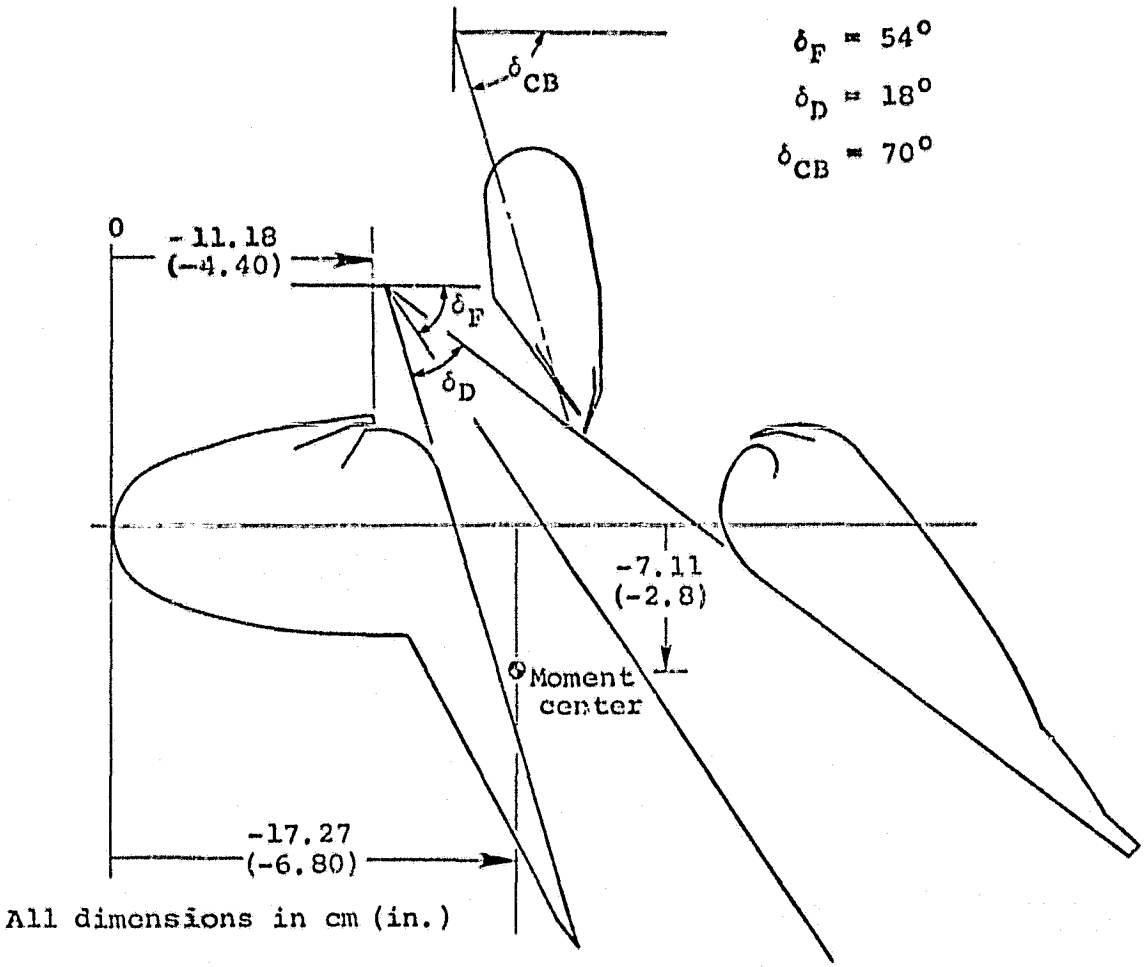

Figure 2.- Chordwise section of transport model augmentor wing of reference 8.

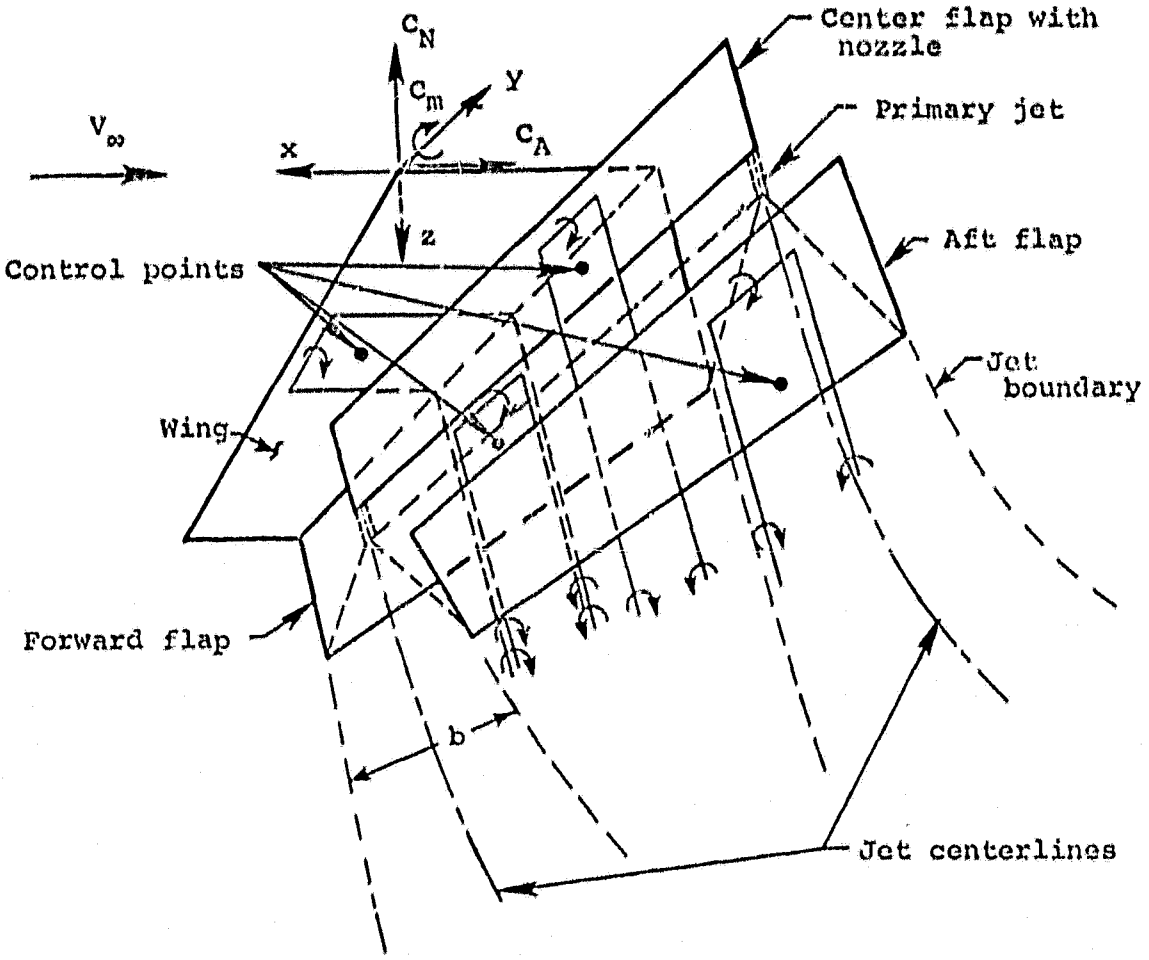

Figure 3.- Chordal planes of an augmentor wing with one horseshoe vortex shown on each surface. Idealized jet centerline and boundaries. Reference coordinate system.

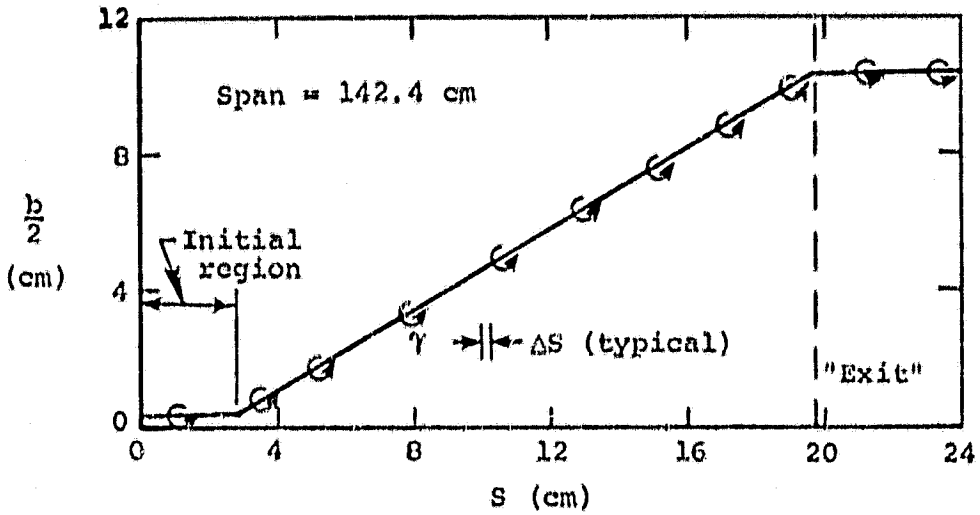

(a) Jet boundary in diffuser region.

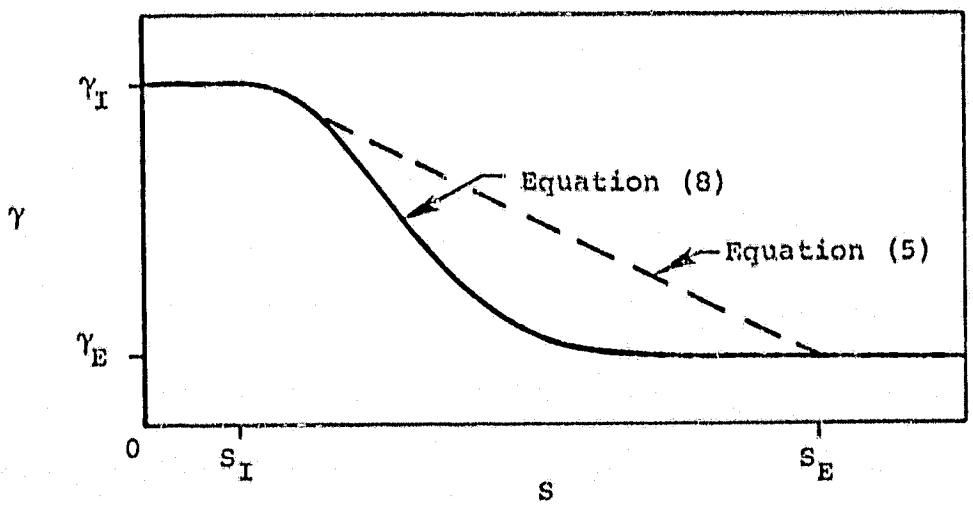

(b) Vortex strength.

Figure 4.- Primary jet model.

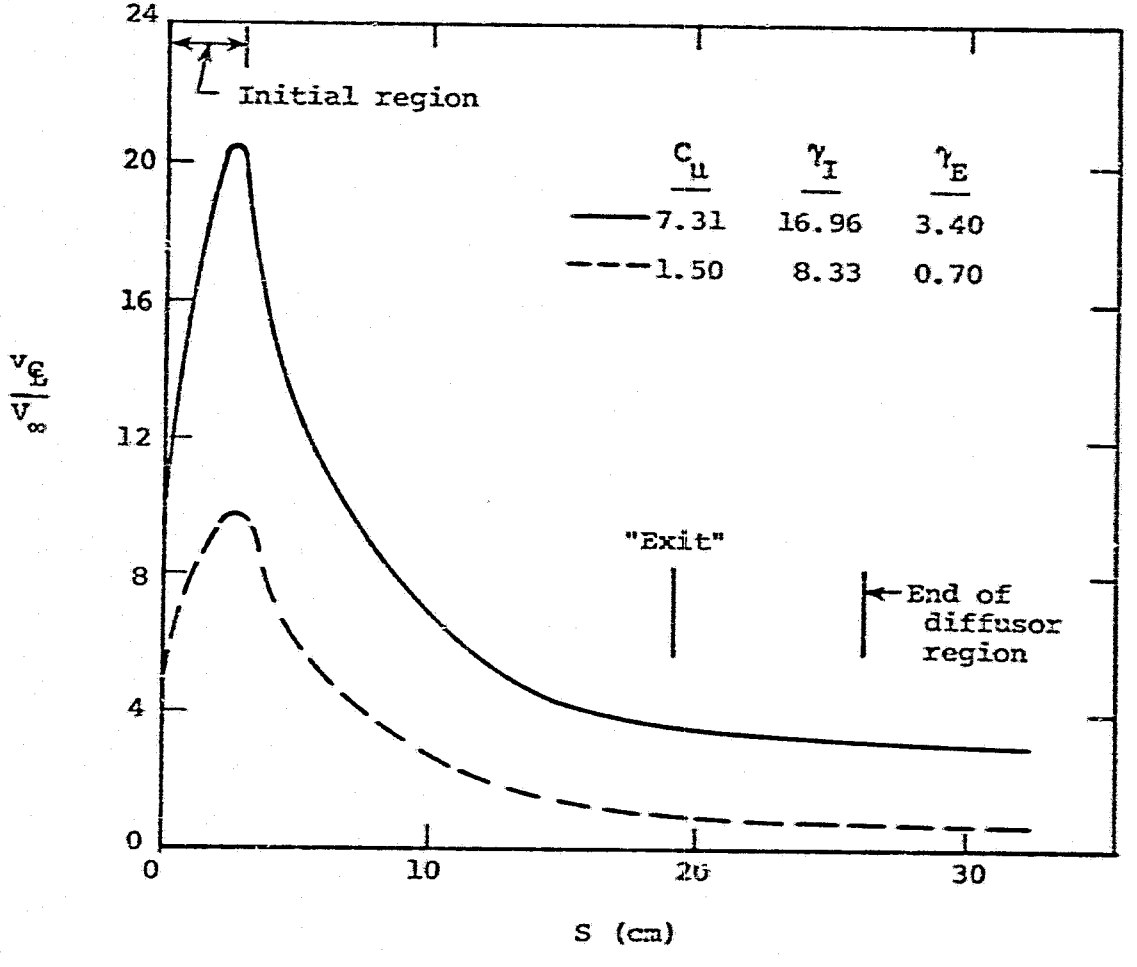

Figure 5.- Primary jet centerline velocity distribution.

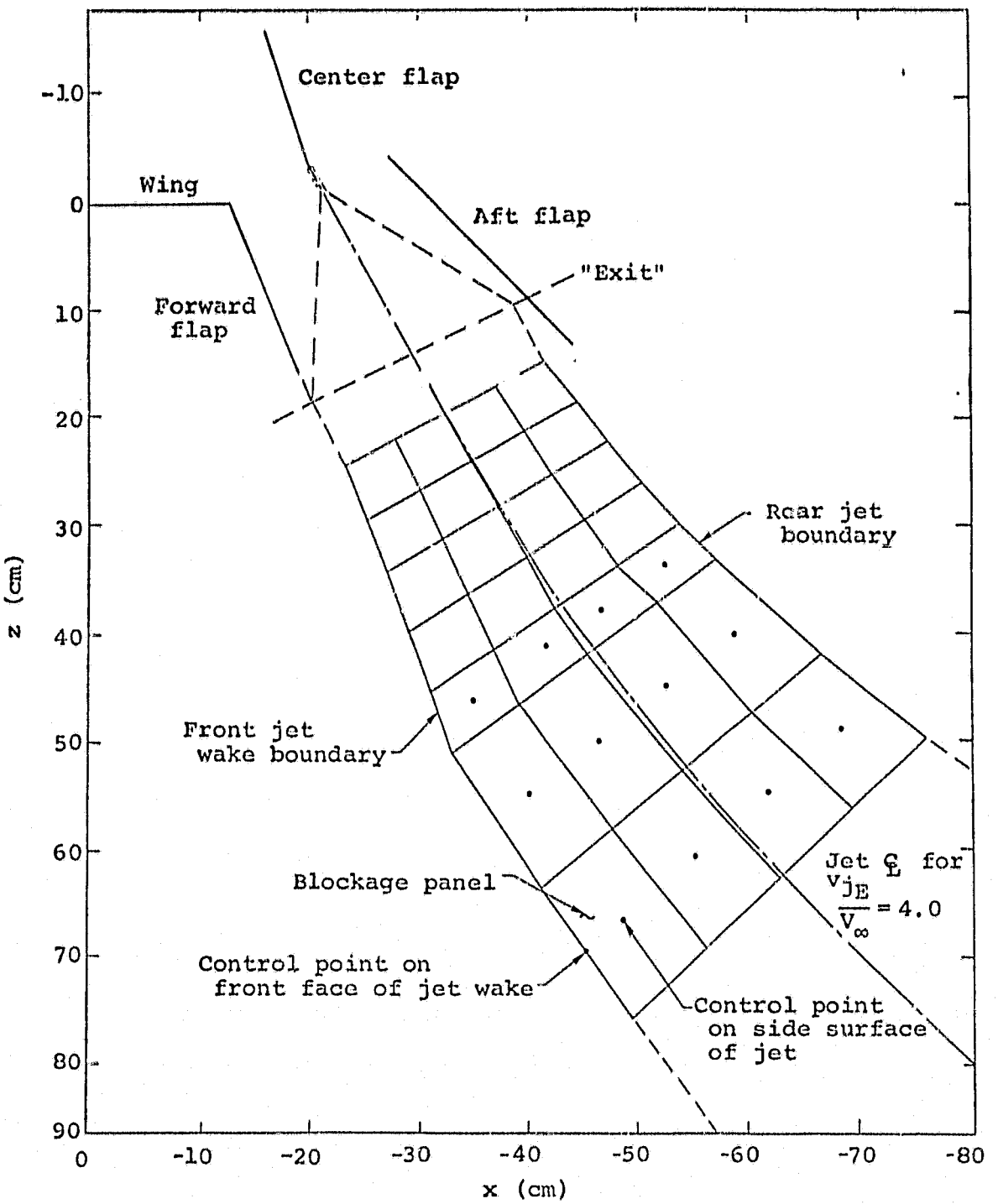

(a) $C_\mu = 7.31$, $\alpha = 0^\circ$.

Figure 6.- Side view of idealized augmentor wing with jet model.

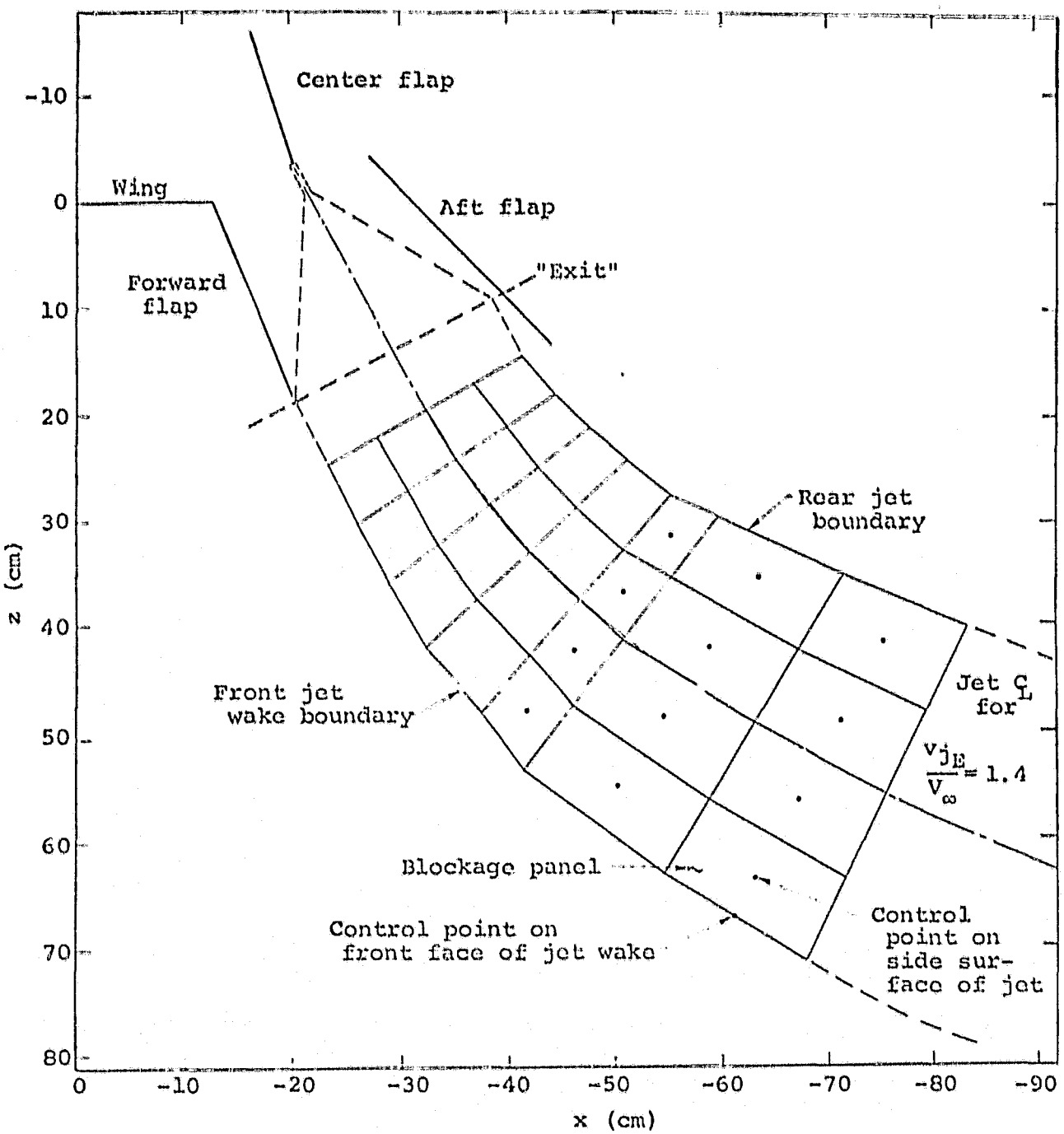

(b) $C_\mu = 1.5$, $\alpha = 0^\circ$.

Figure 6.- Concluded.

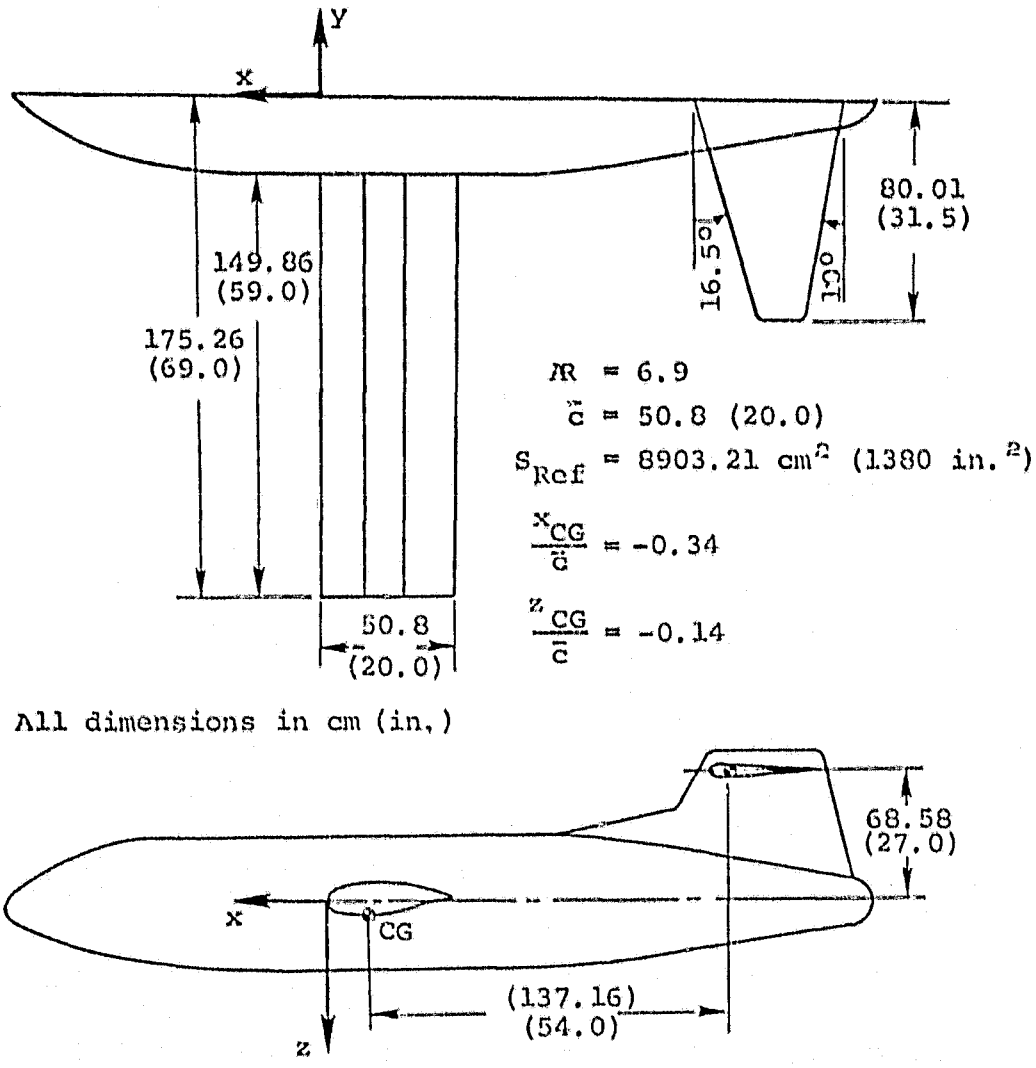

Figure 7.- Rockwell International NACAL 211 Transport Model, references 8 and 15.

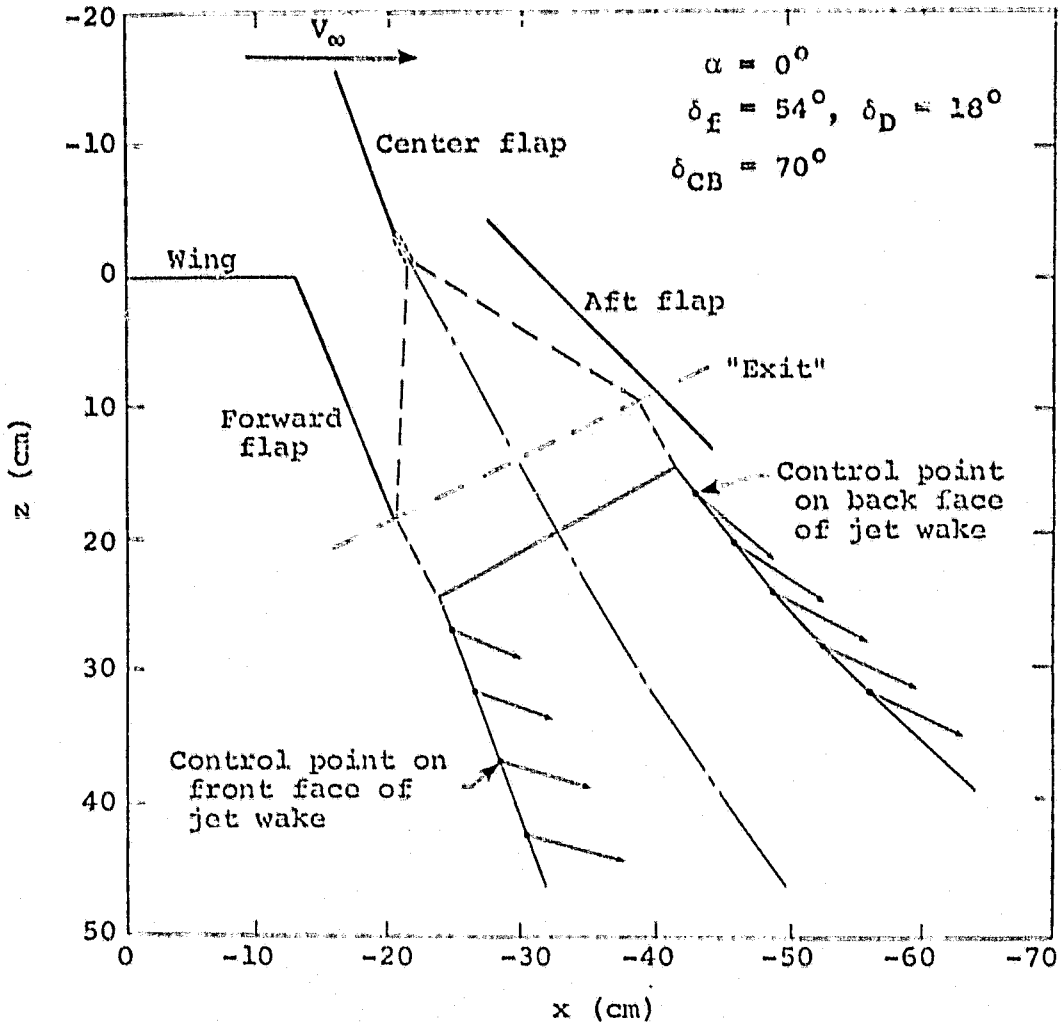

Figure 8.- Velocities induced by vortex lattice on augmentor wing surfaces at control points of blockage panels on upper part of jet wake at y = -103.71 cm (-40.83 in.) spanwise location.

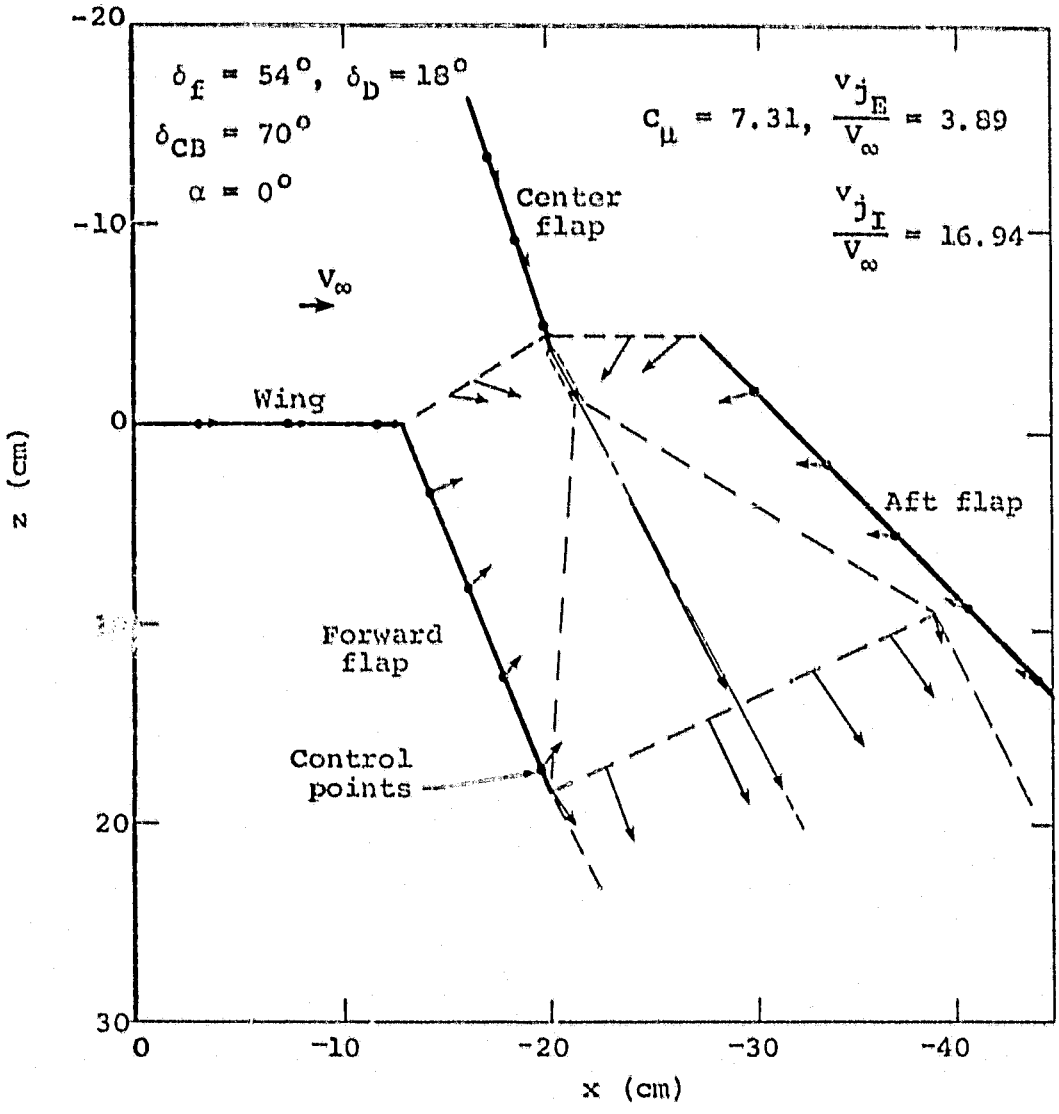

Figure 9.- Velocities induced by jet and jet wake at control points on surfaces of the transport augmentor wing at y = -77.85 cm (-30.65 in.) spanwise location.

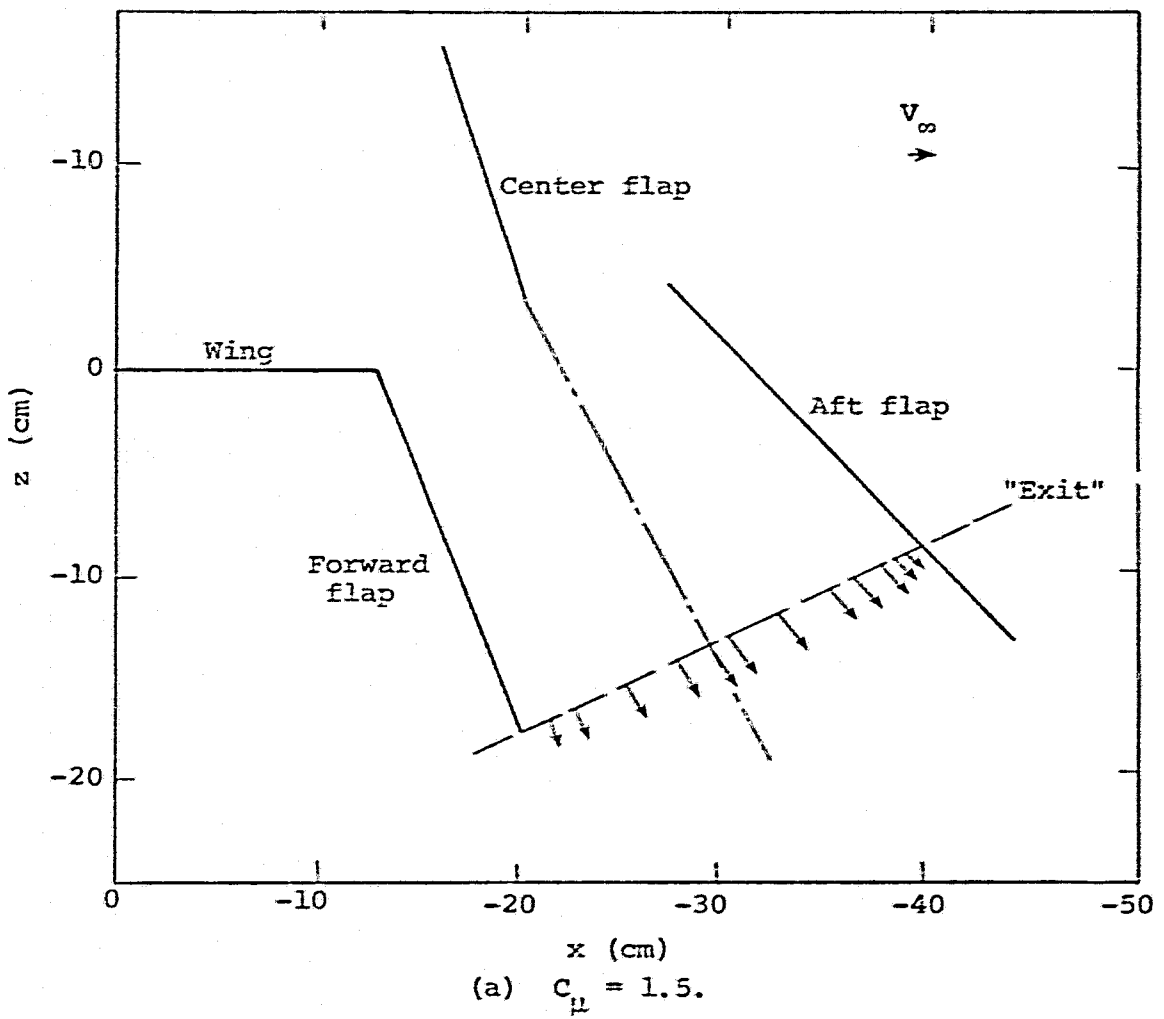

(a) $C_\mu = 1.5$.

Figure 10.- Calculated flow velocities in the diffusor exit at spanwise location y = -74.93 cm (-29.50 in.), $\alpha = 0^\circ$.

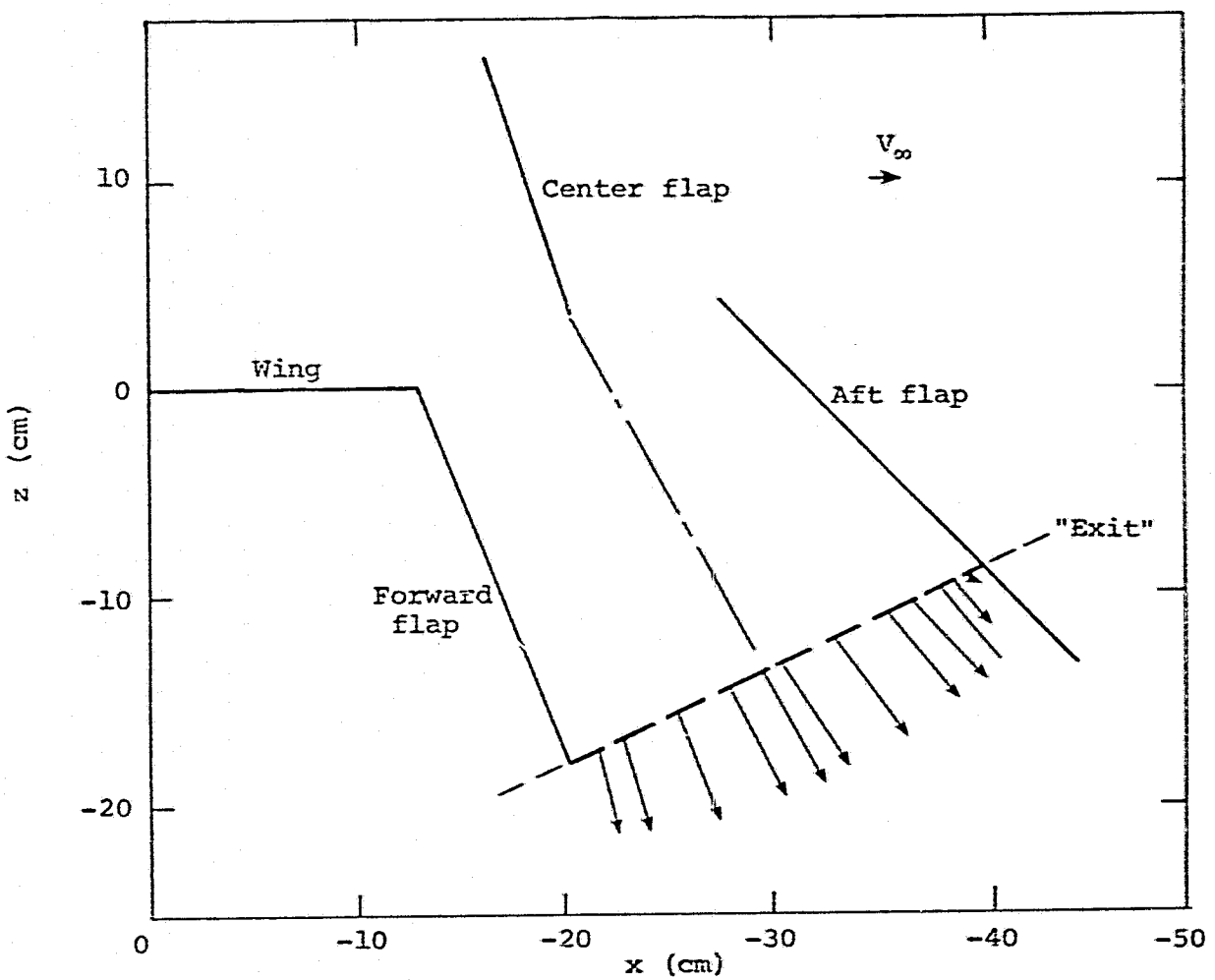

(b) $C_\mu = 7.31$.

Figure 10.- Concluded.

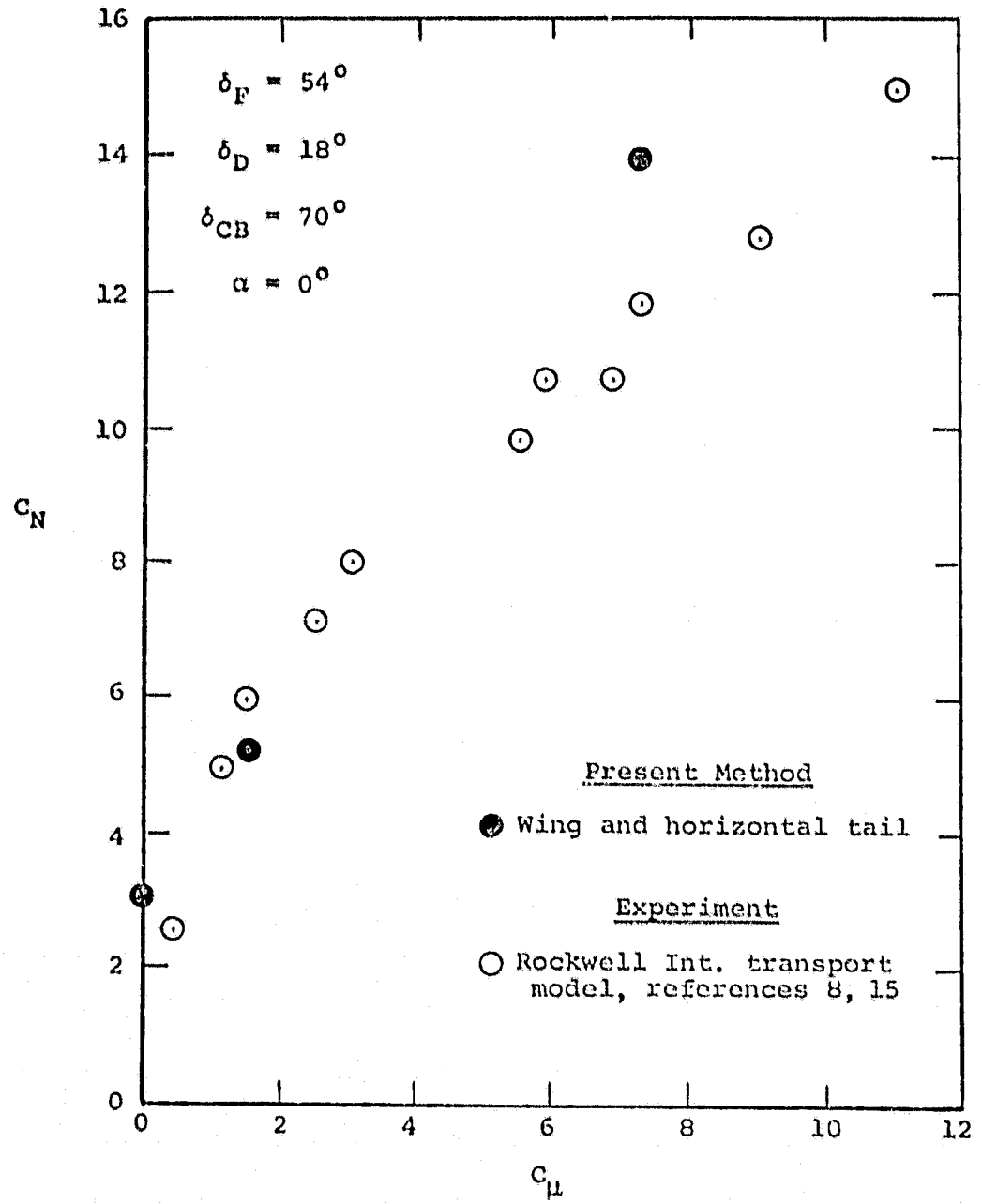

(a) Lift.

Figure 11.- Overall force and moment coefficients as a function of jet momentum coefficient for the NACAL 211 semispan transport model.

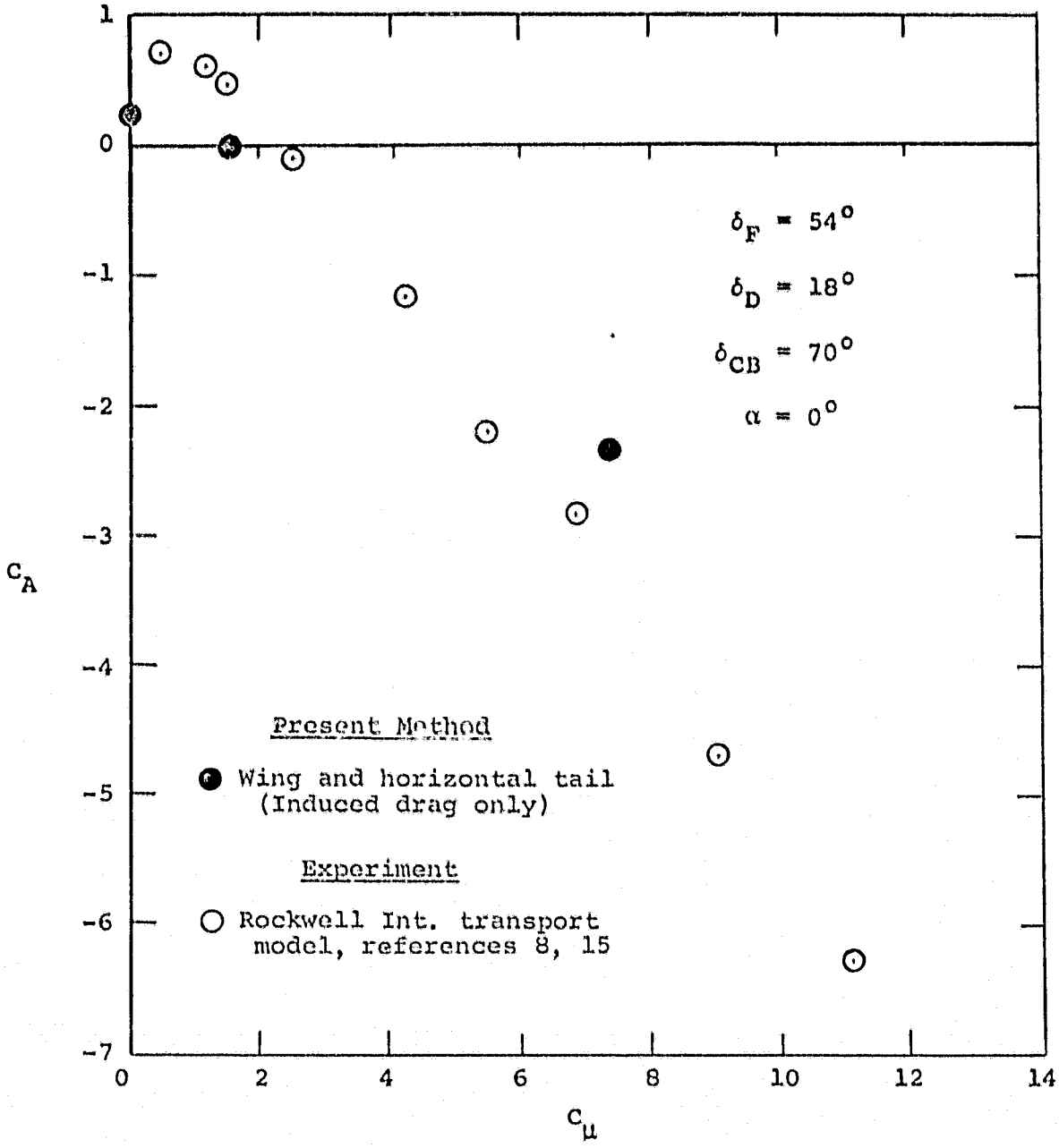

(b) Drag.

Figure 11.- Continued.

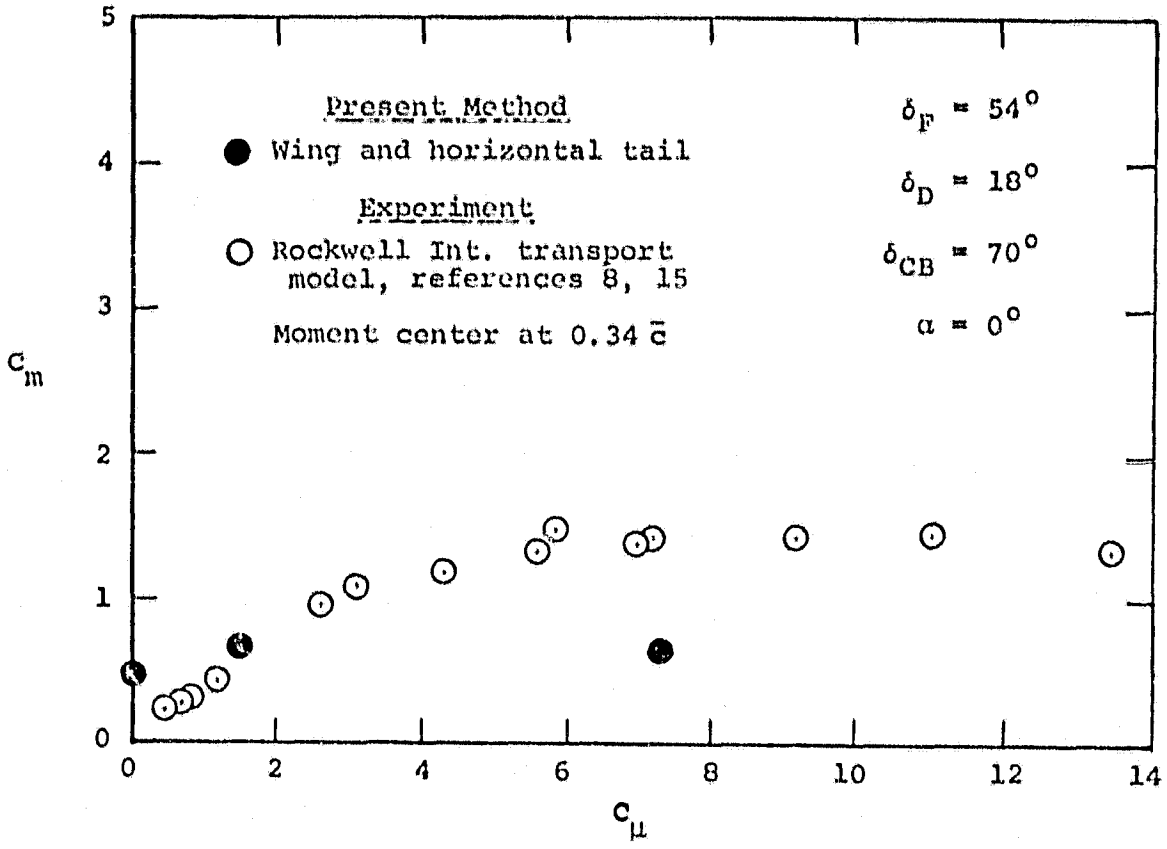

(c) Pitching moment.

Figure 11.- Concluded.

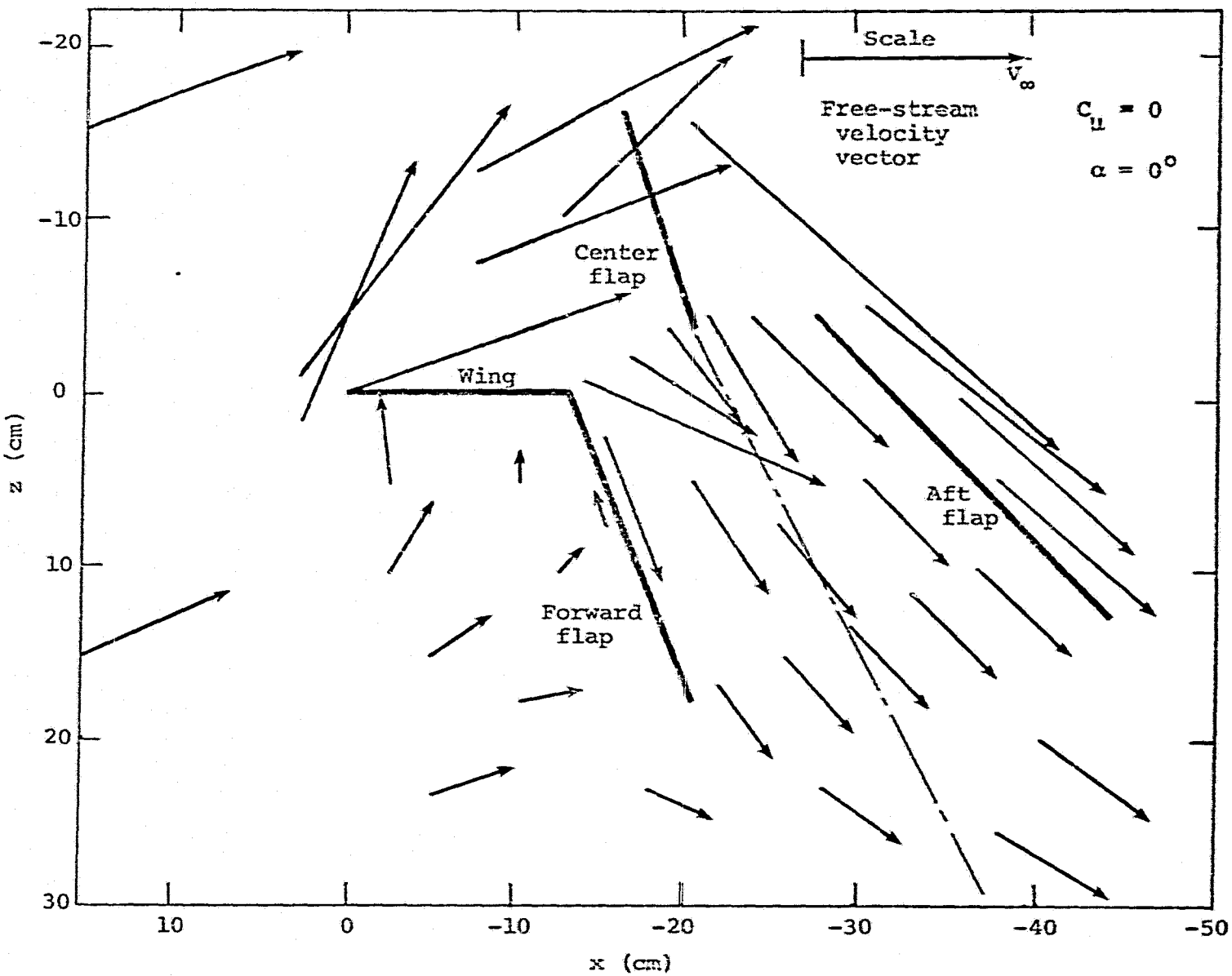

Figure 12.- Calculated flow power-off field in the vicinity of the augmentor wing at spanwise location y = -74.93 cm (-29.5 in.).